




Article

Vehicle Ammonia Emissions Measured in An Urban Environment in Sydney, Australia, Using Open Path Fourier Transform Infra-Red Spectroscopy

Frances A. Phillips ^{1,*} , Travis Naylor ¹, Hugh Forehead ² , David W. T. Griffith ¹, John Kirkwood ³ and Clare Paton-Walsh ¹ 

¹ Centre for Atmospheric Chemistry, University of Wollongong, Wollongong 2522, Australia; naylor@uow.edu.au (T.N.); griffith@uow.edu.au (D.W.T.G.); clarem@uow.edu.au (C.P.-W.)

² SMART, University of Wollongong, Wollongong 2522, Australia; hughf@uow.edu.au

³ Office of Environment and Heritage, Government of NSW, Lidcombe 2141, Australia; John.Kirkwood@environment.nsw.gov.au

* Correspondence: francesp@uow.edu.au; Tel.: +61-242-214-104

Received: 25 February 2019; Accepted: 13 April 2019; Published: 19 April 2019



Abstract: Airborne particulate matter (PM) is a major health risk in urban settings. Ammonia (NH₃) from vehicle exhaust is an under-recognised ingredient in the formation of inorganic PM and there remains a shortage of data to properly quantify the role of NH₃ from vehicles in PM formation. An Open-path Fourier transform infra-red (OP-FTIR) spectrometer measured atmospheric NH₃, carbon monoxide (CO) and carbon dioxide (CO₂) at high temporal resolution (5 min) in Western Sydney over 11 months. The oxides of nitrogen (NO₂ and NO; NO_x) and sulphur dioxide (SO₂) were measured at an adjacent air quality monitoring station. NH₃ levels were maxima in the morning and evening coincident with peak traffic. During peak traffic NH₃:CO ratio ranged from 0.018 to 0.022 ppbv:ppbv. Results were compared with the Greater Metropolitan Region 2008 (GMR2008) emissions inventory. Measured NH₃:CO was higher during peak traffic times than the GMR2008 emissions estimates, indicating an underestimation of vehicle NH₃ emissions in the inventory. Measurements also indicated the urban atmosphere was NH₃ rich for the formation of ammonium sulphate ((NH₄)₂SO₄) particulate was SO₂ limited while the formation of ammonium nitrate (NH₄NO₃) was NH₃ limited. Any reduction in NO_x emissions with improved catalytic converter efficiency will be accompanied by an increase in NH₃ production and potentially with an increase in NH₄NO₃ particulate.

Keywords: ammonia; NH₃; urban; air quality; carbon monoxide; CO; vehicle; particulate matter; open path FTIR spectroscopy; emissions

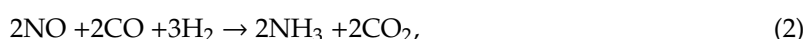
1. Introduction

Fine particulate matter (PM_{2.5}) is recognised as being detrimental to urban air quality and human health [1–3]. The pollutants, primarily responsible for adverse health effects in Sydney, are reported to be PM_{2.5}, PM₁₀, ozone and nitrogen dioxide (NO₂) [4]. The respiratory system is recognised as the main target for harmful effects of pollution, with some evidence for an increase in lung cancer, chronic obstructive pulmonary disease (COPD) and respiratory disease [3]. In addition, a relationship between air pollution and preterm births, has also been suggested [1]. In Sydney, in 2007, it was estimated that PM_{2.5} was responsible for 430 premature deaths or around 2% of total deaths, while 630 respiratory and cardiovascular hospital admissions was attributed to PM_{2.5} and ozone exposure [5]. The main source of PM_{2.5} in the Sydney region, has been shown to be from motor vehicles [6].

In the polluted, urban atmosphere, non-organic PM_{2.5} is produced via the reaction between NH₄⁺ and SO₄⁻² or NO₃⁻¹, with (NH₄)₂SO₄ forming in preference to NH₄NO₃ [7,8]. Ammonia (NH₃) is the only alkaline precursor for the production of non-organic secondary PM_{2.5}, in the urban atmosphere and is often noted as the limiting precursor [7,9]. The main sources of NH₃, in the urban environment, include industrial processes, water and sewage treatment plants and 3-way catalytic converters in petrol vehicles [10,11]. NH₃ is a by-product in the reduction of NO at the catalyst [10,12] and can be the major source of NH₃ in the urban environment [7,10,11,13]. In a correctly functioning 3-way catalytic converter NO is reduced to N₂ on the catalyst via Equation (1) [12].



NH₃ results from the over-reduction of NO in the presence of hydrogen (H₂) [11,12].



The H₂ is provided at the catalyst by a reaction between CO and H₂O [10,11,14]



As NH₃ is not commonly a controlled species in urban environments [10], emissions from vehicles are not closely monitored, with estimates, for inclusion in inventories, typically based on a limited number of measurements, made under controlled operating conditions [12]. Emissions of NH₃ in inventories have been reported to be underestimated by as much as half [12,13,15].

Vehicle NH₃ emissions, from 3-way catalytic converters, can be difficult to quantify as the influences on NH₃ production are complex and varied [16]. Operating vehicles with high fuel to oxygen ratio (“running rich”) [10,11] or below the optimal temperature of the catalytic converter, results in increased NH₃ production [7,17]. Hence emissions are greatest from vehicles in stop-start traffic, involving short bursts of acceleration and the catalyst not reaching optimal temperature [7], in uphill driving [18] or in aggressive high speed highway driving [11,16–18]. Older vehicles can have significantly higher NH₃ emissions (up to a factor of 10) and emission rates may vary with the type of catalytic converter installed, which differs with the make and model of vehicle [12]. Sulphur in the fuel poisons the catalyst, decreasing the catalytic efficiency and inhibits the production of H₂ in Equation (2), resulting in lower NH₃ production and increased vehicle NO emissions [10–12,14]. Improvements in technology have led to decreased emissions of CO and NO_x from vehicles over the previous 10 year but emissions of NH₃ have remained constant, with some Euro 6 compliant vehicles showing increases [11].

The number of studies of NH₃ and related emissions from the urban vehicle fleet is small but interest in the topic has increased over the last 20 years. Studies have included roadside measurements [15,18,19], at exit of road tunnels [13,15,20] airborne measurements [9,21] and tail-pipe measurements [10,14,17]. Measurement technologies included: distribution of NH₃ denuders or absorption techniques [7,13,22], mass spectrometry [17], and, more recently, open path infrared quantum cascade [18,23] and open path Fourier transform infrared (OP-FTIR) spectroscopy [19,24,25]. Many of these techniques can only measure for a limited time or for example, for denuders, with limited temporal resolution. The quantification of NH₃ emissions, within an urban environment, remains limited and consequently the emission factors (EF) are not well defined [15].

The Australian standard for S in fuels is considered high, compared to many other countries, with a limit of 150 mg/L, in unleaded (90 octane rating) fuel and E₁₀ (includes up to 10% ethanol, 95 octane) fuel, the most commonly used fuel in Australia or 50 mg/L in the higher grade premium unleaded (UL) fuel (98 octane). This is compared with a standard of 10 mg/L maximum for the S content of European petrol. A reduction in the S content for Australian fuels has been proposed recently to take

full advantage of vehicles manufactured to higher emission standards [26]. Lower sulphur fuels are anticipated to result in lower NO_x and SO_2 levels but increased NH_3 vehicle emissions, due to reduced poisoning in 3-way catalytic converters. This is anticipated to lead to changes in levels of inorganic $\text{PM}_{2.5}$, dependent on the relative changes in levels NH_3 , SO_2 and NO_x .

The purpose of this work is to quantify a range of gas species relevant to urban air quality with high temporal resolution and an emphasis on NH_3 emissions. Measurements were made in Western Sydney, Australia, over 11 months. While air quality, in Sydney, is generally classed as “good,” exceedances to the air quality guidelines do occur, with the number of exceedances greatest in the west of Sydney. The greater city of Sydney is located within the Sydney Basin, a geographical depression, with the Pacific Ocean to the east and the Great Dividing Range to the west. Typically urban polluted air, from the east of the city, is pushed to the city’s west, by the sea breeze, where it is trapped against the mountains.

The aims of this work were to assess the viability of open-path Fourier transform (OP-FTIR) spectroscopy, for long term measurements of urban air quality; provide quantification of atmospheric NH_3 in an Australian urban environment and provide baseline measurements of NH_3 emissions prior to the possible introduction of lower S fuels.

An extended open-path, mid-infrared Fourier transform (OP-FTIR) spectrometer, simultaneously measuring the mole fraction of infra-red active gases, notably NH_3 , CO , CO_2 and CH_4 , was located at a measurement site in western Sydney, with a measurement path spanning ~400 m between the roofs of two buildings. An open path differential optical absorption spectrometer (DOAS) was also operated side-by-side with the OP-FTIR, with parallel optical measurement paths. Due to technical difficulties, data from the DOAS are not reported here. A Mobile Air Quality Station and an FTIR trace gas analyser, operating adjacent to the spectrometer, provided in-situ measurements, for a range of species relevant to air quality, including $\text{PM}_{2.5}$, NO_x and SO_2 .

We believe this to be the first, direct measurements of NH_3 emissions, in an Australian urban environment and one of the few times OP-FTIR spectroscopy has been used to investigate urban air quality [19,24,25]. CO and CO_2 are produced by the combustion of fossil fuels, with vehicle exhaust being the major urban source of CO and CO_2 . As the majority of urban NH_3 is produced by petrol vehicles, there is a reported strong linear correlation between concentrations of CO and CO_2 with NH_3 [7,9,11,18,19]. The simultaneous measurement of CO , CO_2 and NH_3 by the OP-FTIR allows the CO and CO_2 to act as a tracer for vehicle emissions in the urban environment. The collocation of the Air quality Monitoring station provided complementary information to facilitate source appropriation and chemistry of the measured species. The majority of NO_x and NO_2 emissions originate from diesel vehicles [19,27] and we compare the ratios of NH_3 and NO_x to CO to give a measure of relative emissions from petrol and diesel vehicles. Relative levels of NH_3 , SO_2 and NO_x can provide information on the formation of inorganic particulate matter. The near 12 month record, at high temporal resolution and precision, has afforded us a rare opportunity to compare emissions from a range of sources across time scales from the time of day, to day of week and winter versus summer.

2. Experiment

2.1. Site

The measurement site (Figure 1) was commissioned on the 26 May 2016, on the roof of a two storey building at 2 Percy Street Auburn, in Western Sydney (33.854690° S, 151.037400° E), with the installation of a NSW Office of Environment and Heritage (OEH) Mobile Air Quality Station (MAQ). The site is located 16 km west of the Sydney Harbor Bridge and the city of Sydney’s main business district, with the foothills of the Great Dividing Range and the start of the Blue Mountains, 17 km to the west of the site. (Figure A1). To the immediate west of the Percy St building (25 m) is a major rail line, frequently utilised by heavy diesel freight, for the transport of bulk coal and general freight, plus intra-urban electric passenger rail services. To the west of the rail line is predominantly urban housing. Immediately to the east (330 m) and south (1.2 km), is a major intra-urban road (A6) with a major

intersection 400 m to the north-east. A major inter-urban motor way (M4) and Great Western Highway (A44) is 2.1 km and 2.0 km to the east.

The OP-FTIR spectrometer system was installed, adjacent to the OEH MAQ station, on 28 October 2016 and operated until 13 September 2017. The system did not operate between 17 March and 23 May 2017, to allow for maintenance. The Spectrometer was housed in a small shed, for weather protection. The retroreflector array, terminating the measurement path of the spectrometer, was located on the roof of a three story, Auburn City Council, building at 2 Susan Street (33.85311° S, 151.0335° E) (Figure 1). The distance between the two buildings is approximately 400 m and spans the railway line. The Council building is within the Auburn business district, on top of a small hill. The roof top of the Percy St building is 6.72 m above ground level, 20.6 m above sea level and the Council building 12.8 m about ground level, 40.8 m above sea level, with a difference in altitude between the two building roof tops of 20.2 m.

For the analysis, data have been divided into “summer” (October 2016 to March 2017) and “winter” May 2017 to September 2017. While this reflects the warmer versus cooler months, it also divides the data between daylight-savings (Australian Eastern Daylight Time (2 October 2016 to 2 April 2017 (AEDT, UTC + 11) and Australian Eastern Standard Time (3 April 2017 to 1 October 2017 (AEST, UTC + 10)). While all times are recorded as AEST, the hour difference with AEDT is reflected in traffic peak hours and industry operating hours. Data for the site are available at [28].



Figure 1. The measurement site at the edge of the Auburn business district. The location of the main measurement site including the open path Fourier transform infra-red (OP-FTIR) spectrometer location (□), on roof of 2 story building and retro-reflectors (★) on roof of 3 story building at the edge of the small business district in Auburn is located. The measurement path (395 m) is marked (-). There is a major intersection in the north-east. To the east is light industrial area, with mainly residential to the east. The measurement path crosses a railway line and a major intra-urban motorway is to the east (not shown on the map).

Vehicle Fleet Statistics

The light passenger vehicle fleet, in 2016–2017, was predominantly petrol, accounting for 94% of the fleet. Diesel vehicles are less popular in Australia compared to Europe and account for 5% of the fleet with electric, dual electric/petrol and gas powered vehicles making up ~1%. The average age of vehicles in the region of the measurement site is 10 years. This is typical in Australia [29].

The inter-urban M4, 2.1 km to the east of the site, was a 2 × 2 lane freeway, until July 2017 when extra lanes were added, to 3 × 3 lanes. The speed limit of the M4 is 90 km h⁻¹. The A44, 1 km to the east of the site and running parallel to the M4, is an intra-urban/local 2 × 2 lane local road with 50 km h⁻¹ speed limit. The A6, 400 m to the east and 1.2 km to the south, is a 2 × 3 lane, intra-urban road with 70 km h⁻¹ speed limit. The intersection on the A6, 400 m to the northeast of the site, is controlled by traffic lights, with the major traffic flow turning 90°, at the intersection. The general direction of the A6 is cross-city, north-south. The direction of the A44 and M4 is east-west, radial to the city.

Estimates for number of trips on the A6, A44 and M4 are included in Table 1. Vehicle trips were sourced from camera-counters, for each road [30], for each hour of the day and each month and averaged to a daily distribution. The distribution over the day is presented in Figure A2. On the A6, light passenger and heavy vehicle traffic statistics were available in 2016–2017, for north bound lanes only, from camera-counter (counter 7112), ~1 km from intersection on the A6, close to the M4 interchange. A second camera-counter (50,206), ~4 km north of the intersection, monitored A6 north and south bound traffic. While numbers were higher at 50,206 compared with 7112, the number of north and south bound vehicles, at 50,206, were similar, and, the distribution on the north bound lane was similar to that at 7112. Based on this, north bound statistics at 7112 have been used for south bound statistics. On the A44, camera-counter (47,024) monitored east and west bound traffic ~1.4 km east of the A6/A44 intersection. For the M4 very limited statistics are available. Camera-counter (48,001) ~1.8 km east of the A6/M4 interchange, provided statistic for east-west bound and light and heavy vehicles, for 5 months during 2014–2015. From mid-2017, daily, total numbers are available. Daily, east-west and heavy-light vehicle distribution has been taken from the 2014–2015 statistics and adjusted to 2017 total numbers (~11% increase in traffic numbers).

Table 1. Traffic Statistics, average trips per day, for the major roads, A6, A44 and M4, to the east of the measurement site. Statistics have been taken from the camera-counters monitoring road traffic on each road.

	Light Vehicles		Heavy Vehicles		Total Light	Total Heavy
	North or East	South or West	North or East	South or West		
Week days						
* A6	19,779	19,779	2193	2193	39,558	4386
A44	149,760	155,226	15,676	18,541	304,986	34,217
** M4	67,702	64,908	8544	7493	132,609	16,037
Weekend						
* A6	18,037	18,037	712	712	36,074	1424
A44	118,203	141,734	3811	5464	259,937	9275
** M4	56,244	63,102	2970	2385	119,346	5355
Total Trips						
Week days	237,241	239,913	26,413	28,227	477,153	266,325
Weekend	192,484	222,873	7493	8561	415,357	16,054

* Numbers from A6 north bound have been used for A6 south bound statistics, based on statistics from a counter. ~3 km further north, 4 km from the intersection on the A6. ** Statistics for M4 have been taken from 2014/2015 data and adjusted for 2017 total numbers.

On weekdays, traffic on the A6 peaked at 7:00 a.m. (north bound) and 17:00 (south bound). Peak traffic on the M4, was less distinct, with maximum between 5:00 and 8:00 and 16:00 and 18:00. Similarly, on the A44 peak traffic was between 6:00 and 8:00 and 15:00 and 18:00. On weekends, light vehicle traffic was more evenly distributed during the day, increasing from ~9:00 until ~17:00. Heavy vehicle traffic, during the week, was distributed more evenly over the day, from ~5:00 to 18:00 but decreasing from ~15:00, with heavy vehicles trips, during the afternoon traffic peak, ~ 50% of trips during the morning peak traffic. On weekends, the number of heavy vehicle trips was ~ 30% of weekday trips. Traffic speed data were not available, however, based on Google Typical Traffic for the area, the A6 is slow from 7:00 to 10:00 and again 16:00 to 18:00; the A44 is slow from 7:00 to 10:00, slow at 16:00, congested and very slow from 17:00 to 18:00 and free flowing from 19:00. The M4 was reported as very slow during peak times, until the opening of the additional lanes, after which traffic was free flowing.

2.2. Instrumentation

2.2.1. Open Path Infrared Fourier Transform (OP-FTIR) Spectrometer

The OP-FTIR system continuously measures the mole-fraction of infrared active gases, including CO, CO₂, CH₄ and NH₃, between the spectrometer and the distant retroreflector, which define the ends of the measurement path. The OP-FTIR has previously been used extensively to measure gaseous emissions (CO, N₂O, NH₃ and CH₄) from agricultural systems [31–37], simulated leaks from coal-seam gas wells [38] and emissions from vegetation fires [39,40].

In this work the length of the one-way measurement path, between the spectrometer and retroreflectors, was 395.8 m (measured by GPS to ± 0.5 m) and varied from 7.9 m to 15.2 m above ground level between the Percy St building and the Council building. The height of the measurement path above the Percy St roof-top was 1.2 m and 2.4 m above the council roof top at the retroreflector corner cube array, with a difference in the height above sea level of the two ends of the measurement path of 21.4 m.

The OP-FTIR system is illustrated schematically in Figure 2 and consists of a mid-infrared FTIR spectrometer (global source, ZnSe beamsplitter, 1 cm⁻¹ resolution, Matrix IR-Cube, Bruker Optik GmbH, Ettlingen, Germany) to provide a parallel 25 mm modulated infrared beam. The modulated beam from the interferometer is transmitted through an external ZnSe beam-splitter (50 mm diameter \times 3 mm) to a beam expander that expands the beam to 250 mm and decreases the divergence by a factor of ten to 2 milliradians. The beam expander consists of a modified Schmidt Cassegrain telescope (LX 200ACF, Meade Instruments Corporation, Irvine, CA, USA) with the Schmidt corrector plate removed and the secondary mirror replaced by a convex mirror with effective focal length of 50 mm and virtual focus collocated with the focus of the primary mirror. The spectrometer, beam-splitter, modified telescope and secondary mirror are mounted on an optical rail that defines the instrument's optical axis. The outgoing expanded beam is focused on the remote retroreflector array by moving the secondary mirror on the rail along the optical axis. The outgoing beam is terminated by a 3 \times 30-cube gold coated hollow corner-cube array (PLX Industries, New York, NY, USA) which returns the infra-red beam to the primary mirror of the telescope, the secondary mirror and the external beam splitter where half the beam intensity is reflected to a 90° off axis parabolic mirror and focused onto a Mercury Telluride Detector (MCT; Infrared Associates Inc., FL, USA or Judson Industries, Montgomeryville, PA, USA) cooled to 78 K (−196 °C) by a sterling cycle mechanical cooler (Ricor K508 micro-cooler, RICOR, Nashua, NH, USA). The transmitted half of the beam from the beamsplitter returns to the spectrometer, offset from the output beam by the retroreflectors. To prevent the return beam from re-entering the spectrometer a half-mask is installed at the input side of the spectrometer window.

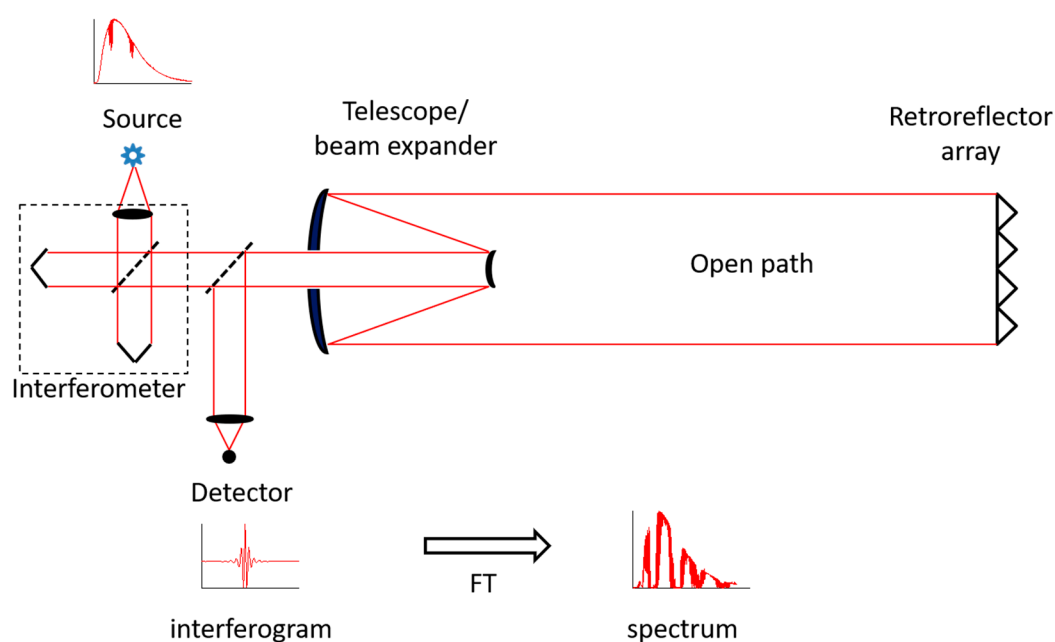


Figure 2. Schematic optic diagram of the open path FTIR system.

A small mask (optically black disc, approx. 3 mm in diameter) is installed at the centre of the secondary mirror, to minimise the direct back-reflection of the output beam, from the centre of the secondary mirror, back to the beam-splitter, detector and spectrometer. This direct back reflection does not transverse the open atmosphere, between the spectrometer and retro-reflector array but contains the spectrum of the atmosphere, between spectrometer and secondary mirror, which is superimposed on the main long path spectrum. While the intensity of back-reflection spectrum is small and constant, the relative intensity of the two spectra varies with variation in the intensity of the main spectrum, due to changing atmospheric and spectrometer conditions. Any residual back reflection spectrum from the secondary mirror is fitted and subtracted from the recorded total spectrum before spectrum analysis to retrieve concentrations over the long open path.

The OP-FTIR optical rail is mounted onto a heavy duty tripod (Gibraltar model 4-60450-OA, Quickset International Inc., Northbrook, IL, USA) via a computer-controlled Automated Instrument Mount (AIM; OmegaLec Pty Ltd., Unanderra, Australia) that allows accurate alignment to retroreflector arrays and programmable rotation between up to a maximum of 6 reflectors. The global source produces CO within the spectrometer and, as CO was an important target gas in this work, the spectrometer was purged with N₂ gas (instrument grade, BOC Australia, Sydney, Australia). Temperature and pressure, required for the spectral analysis, are measured by a Vaisala barometer (PTB110, Vaisala Oyj, Vantaa, Finland), located at the spectrometer and LM335 temperature diode housed in a Stevenson's screen approximately 2 m from the spectrometer, at the height of the measurement path and away from any shadowing. The 21.4 m difference in height above sea level of the retroreflector and the FTIR and pressure sensor correspond to an approximate 2.5 hPa lower pressure; measured pressures were decreased by 1.2 hPa to obtain a path-mean pressure.

The measured spectra are analysed by the program MALT (Multiple Atmospheric Layer Transmission) [41–43] using a nonlinear least squares fit of the measured spectra to synthetic spectra, generated by the program. MALT analyses the spectra immediately after collection, in user defined spectral windows. Inputs to MALT include spectral line parameters for all identified absorbing species within the window, plus parameters for fitting the spectral line width, asymmetry and wavelength shift and a polynomial term to account for the underlying continuum spectrum. In this work the spectral line parameters, for all absorbing species, were sourced from the HITRAN04 database [44]. The spectral windows and the gas species included in the spectral analysis, are given in Table 2. Examples of fits of

the synthetic to measured spectra are shown in Figure 3. Other species, including methanol, SO₂, NO₂, formaldehyde, formic acid, acetylene, ethylene and ethane were identified in spectra collected when smoke haze was present and air quality was poor and are reported in Reference [45].

Spectra were collected as 5 min averages, less 8 s to allow for the MALT spectral analysis (730 co-added spectra). The system ran autonomously, with data downloaded hourly to an off-site server and spectral quality checked remotely. Maintenance checks, including cleaning any exposed optics and replacing the N₂ purge gas bottle, were performed every 2 to 3 weeks.

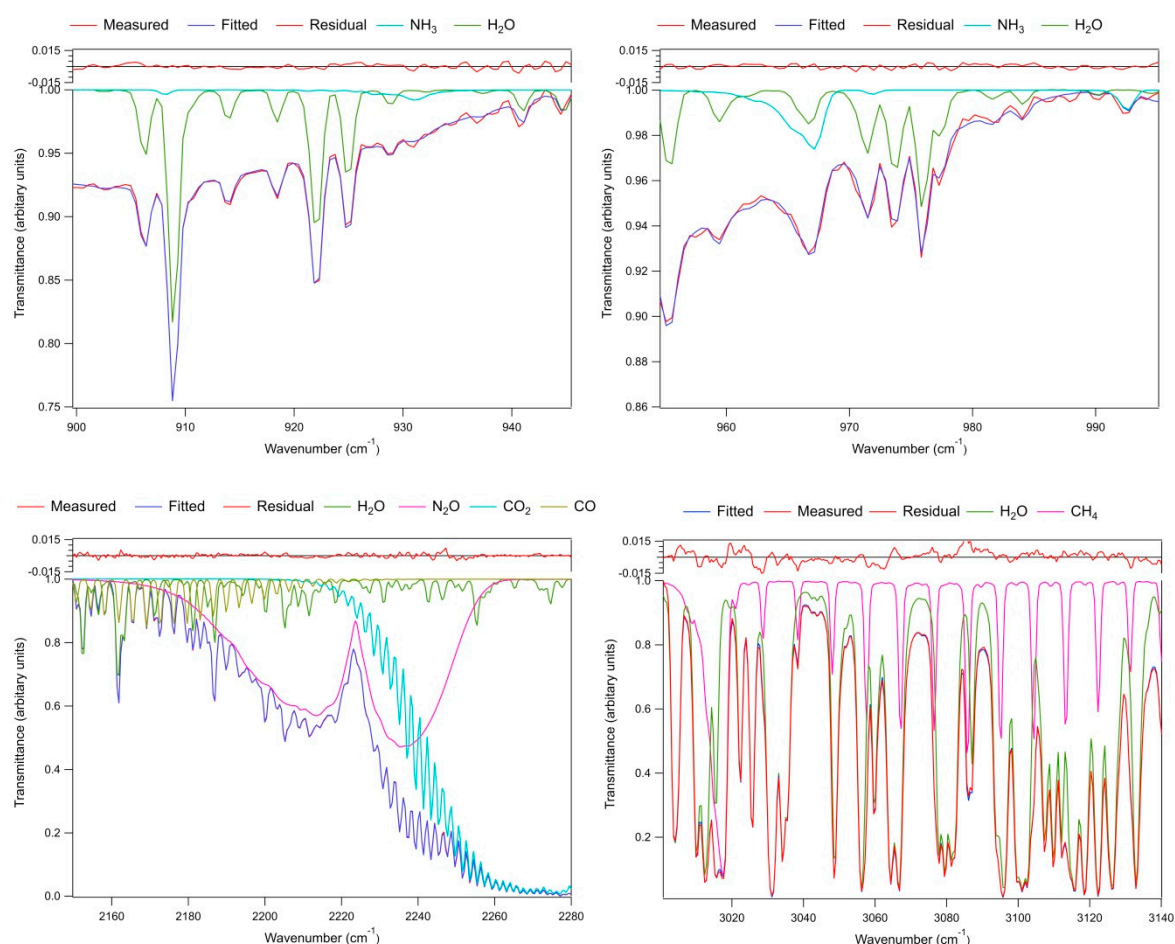


Figure 3. Shows examples of the fit of the modelled synthetic spectrum to the measured spectrum and the resulting rms residual for: top left panels NH₃ in the 900 micro-window and right panel in the 955 cm⁻¹ micro-windows; lower left panel CO₂, N₂O and CO in the 2300 cm⁻¹ micro-window; and lower right panel CH₄ in the 3000 cm⁻¹ micro-window.

Table 2. Spectral Micro-windows limits used for the Multiple Atmospheric Layer Transmission (MALT) analysis of the OP-FTIR spectra.

Target Gas Species	Micro-Window Wavelength Limits (cm ⁻¹)	Interfering Species
* NH ₃	900–945, 955–995	H ₂ O
CO, CO ₂ , N ₂ O	2150–2280	H ₂ O
CH ₄	3001–3140	H ₂ O

* Analysis for NH₃ was divided between 2 micro-windows to avoid a spectral artefact.

2.2.2. In situ Trace Gas Analyser

Data from the OP-FTIR system were verified by comparison against in situ data from an FTIR trace gas analyser built at UoW as an early version of the Spectronus analyser (Ecotech, Melbourne Australia, [42]). This analyser sampled air at an intake ~5 m from the FTIR spectrometer and at a height of 3.3 m above the roof top. The instrument was calibrated prior to deployment against 4 calibrated gas standards (CSIRO GasLab, Aspendale, Australia). To define any drift in calibration during operation, a target gas (11 L aluminium SCUBA tank, filled with air and calibrated against the same gas standards) was measured (20 samples) every 26.5 h. The in situ analyser reported the 1-min average mole fraction for CO₂, δ¹³C in CO₂, CO and N₂O. It operated at the site between 16 July 2017 and 12 September 2017.

2.2.3. Mobile Air Quality Station (MAQ station)

The Mobile Air Quality station was operated by the NSW Office of Environment and Heritage (OEH). The instruments included in the station and the species measured, are detailed in Table 3. The instruments were housed in an environmental enclosure (size 1.4 m × 1.2 m × 1.6 m) equipped with an air conditioning unit to maintain operating temperature. The instruments were calibrated according to NSW EPA standard procedures. Data are reported as the hourly-average of the recorded 1-min measurements. The air quality monitoring station operated from 23 May 2016 to 12 September 2017. These data are presented further in Reference [46].

Table 3. Instruments included in the Mobile air quality station and the gas species analysed.

Species	Instrument	Reference
NO _x , NO ₂ , NO	Teledyne T204 analyser	Teldyne API, San Diego, CA, USA
CO	Teledyne T300	Teldyne API, San Diego, CA, USA
SO ₂	Teldyne Model 100T	Teldyne API, San Diego, CA, USA
PM _{2.5} , PM ₁₀	ThermoFisher 1405-DF TEOM	ThermoFisher Scientific, Waltham, MA, USA 02451
Neph 450, 635, total	Ecotech, AURORA 3000 Integrated Nephelometer	Knoxfield Vic 3180, Australia
Wind speed, direction	Met-One MET505	Met-One, Grants Pass or 97526, USA
Temperature, Humidity	Vaisala HMP155	Vaisala, Helsinki, Finland

2.2.4. Meteorological Data

Wind speed and direction, plus air temperature and humidity, were measured at the Mobile Air Quality Station (Table 3) on the top of the Percy St building. A sonic anemometer was installed on 6 July 2017, extending approximately 1 m over the edge of the Percy St building roof, to provide additional measurement of wind speed and direction plus information on atmospheric stability. The orientation of the anemometers was determined by GPS. Data from the two weather stations were compared with data from the Australian Bureau of Meteorology (BoM) Homebush station, 4 km to the north east of the Auburn site (station number 066212, −33.8338, 151.0718).

3. Results and Discussion

3.1. Meteorological Data

During summer, the wind was predominantly, 63% of the time, coming from the east, from the more industrial area and major roads and 34% of the time from the west and the predominantly residential area. During winter, the wind was coming predominantly, for 87% of the time, from the west and from the east for only 13% of the time. (Figure 4).

Wind speeds measured on the roof of the Percy St building, were generally low, between 2 and 4 m s⁻¹, with higher wind speeds of 4–8 m s⁻¹ from June to September. Wind speeds, measured by the two anemometers, located at the site, were in close agreement but were half that measured at height 10 m, at the Australian Bureau of Meteorology Homebush Station. Wind speeds were usually lowest in the evening, increasing at dawn and greatest in the early afternoon.

Minimum daily temperatures ranged from 14 to 16 °C during summer and 5 and 10 °C in winter. Maximum daily temperatures, in winter, were generally between 15 and 20 °C but exceeded 25 °C on 3 days during August–September. During summer, maximum temperatures ranged from 20 °C to 40 °C, with 6 days exceeding 40 °C. A maximum temperature of 44 °C was recorded at the site on the 10th February.

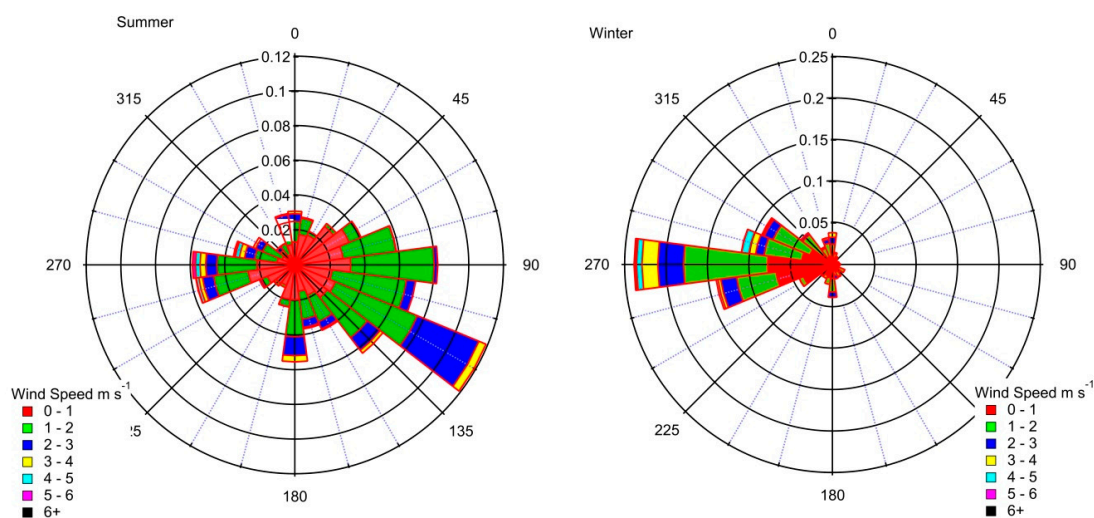


Figure 4. Wind direction and speed measured at the site on the roof of the building from October 2016 to March 2017 (summer) and May 2017 to September 2017 (winter).

3.2. Uncertainty Analysis OP-FTIR Data

An uncertainty budget was calculated for the spectral analysis of CO₂, CO, CH₄ and NH₃, as per Smith et al. 2010 [47] and Paton-Walsh 2014 [39], who reported sensitivity analysis for OP-FTIR/MALT systems similar to that used here. Uncertainties in temperature, pressure, field-of-view (FOV) of the instrument and the choice of polynomial were considered.

While the strength of the absorption lines is temperature dependent and the line-shape is influenced by temperature and pressure via Doppler and pressure broadening, the greater influence of temperature and pressure is in determining air density used to calculate the gas mole-fraction. Temperature and pressure were only recorded at one end of the measurement path, at the spectrometer on the roof of the Percy St building. Based on the comparison of temperature recorded at the spectrometer, the nearby Mobile Air Quality Station and the Bureau of Meteorology sites at Homebush (4 km to north-east) and Bankstown (8 km to the south), a 3 °C uncertainty in temperature was estimated. Systematic uncertainty in pressure due to the sensor accuracy and correction for mean path height above sea level is conservatively estimated to be 2 hPa.

The sensitivity in the retrieval of the gas mole-fraction to the temperature and pressure, determined from the difference in retrieval (Table 4), was similar to that reported by Smith et al. 2010 [47]. Uncertainty for CO and CO₂ estimated by Smith et al. 2010 due to error in the FOV are used in Table 4. As NH₃ was not included in analysis by Smith or Paton-Walsh, a sensitivity analysis compared retrievals using a fixed, 22 mrad and fitted FOV. While the FOV fitted for the 2300 and 3000 cm⁻¹ regions was consistent at ~22 mrad, the fitted FOV for the NH₃ regions was more varied and closer to 30 mrad. The sensitivity of the NH₃ analysis to FOV was similar to that found by Smith et al. 2010 for CO, CO₂ and CH₄. From Table 4 the error in the spectral retrieval is dominated by the systematic

error, in particular the uncertainty in the HITRAN line parameters. The random error in the retrieval is dominated by the quality of the fit to the spectrum. It should be noted the high relative error in the spectral fit for NH₃ is a reflection of the low background levels of NH₃ being measured.

The MALT fit to the spectrum returns two measures of the quality of the analysis, the rms residual for the spectral fit and an error for the spectrum fit for each gas, which is proportional to the rms residual and an upper limit to the true standard error [47]. HITRAN04 was used in the analysis for all gas species in this work. HITRAN04 achieved the lowest reported errors and rms residuals for CO₂, CO, N₂O and NH₃. In contrast, for CH₄ and the 3000 cm⁻¹ region, HITRAN12 parameters gave the lowest reported errors and rms residuals. However, the difference in the retrieved CH₄ and CO mixing ratio using the 3 databases (HITRAN04, 08 and 12) was less than 1%. For CO₂ the difference between HITRAN04 and HITRAN12 was up to 5%. The difference for the NH₃ retrieval using HITRAN04 compared with HITRAN08 or HITRAN12 was +4.8% and -4.8% respectively. The uncertainty in the measurement path is also included in Table 4. The total uncertainty is added in quadrature.

Table 4. The error in the mole-fraction of CO₂, CO, CH₄ and NH₃ retrieved from OP-FTIR spectra using the MALT forward model, including errors arising from the use of an incorrect polynomial and Field of view (FOV) plus the uncertainty in the measured temperature, pressure and path-length, input into MALT to model the measured spectrum. The error due to an incorrect FOV and polynomial for CO₂, CO, CH₄ has been taken from Reference [47]. Systematic (sys) and random (rand) errors are reported separately. The uncertainty in the parameters in HITRAN is included in the database. The total is added in quadrature.

Error Source	Relative Error (%)							
	CO ₂		CO		CH ₄		NH ₃	
	Sys	Rand	Sys	Rand	Sys	Rand	Sys	Rand
Pressure (2 hPa)	0.2	0.05	0.4	0.1	0.2	0.05	0.3	0.1
Temperature (3 °C)	0.3	0.03	1.4	0.1	0.9	0.1	0.7	0.1
polynomial	0.9 *	-	0 *	-	1.0 *	-	1.0	-
FOV	1.8 *	-	5.4 *	-	1.2 *	-	1.4	-
Path-length	0.25	-	0.25	-	0.25	-	0.25	-
HITRAN	5	-	2	-	5	-	5	-
Spectrum fit		0.30		1.0		1.0		13
Total	5.4	0.31	5.9	1.0	5.3	1.0	5.4	12.9

* values for polynomial are taken from Reference [47].

3.3. Validation of OP-FTIR Data

Data from an open-path sensor is not easily calibrated, particularly over the extended path length used here. The repeatability of the OP-FTIR system (Table 5), with the one-way measurement path of ~400 m, was determined as one-standard deviation in the mole-fraction, measured under clean turbulent conditions, over >2 h, for 5-min averaged measurements. Comparing the repeatability of the measurements, relative to the background for each gas (Table 5), with the random error due to the spectrum fit, in Table 4, suggests the repeatability of the measurements for CH₄ and CO₂ are dominated by the quality of the spectral fit, while for CO and NH₃ the RMS noise includes fluctuations in the urban atmosphere being measured.

In the instrument configuration used in this work, signal at the detector was reduced by ~50%, compared to optimal fill of the infrared beam to the reflector, largely due to the divergence of the infrared beam over 400 m. Higher precision is possible with a larger telescope to reduce beam divergence and one or more additional corner-cube arrays to capture a greater portion of the beam.

To validate the OP-FTIR measurements the measured mole-fractions for CO, CO₂ and CH₄ were compared with data from the collocated, calibrated, in situ analyser. Data collected when wind speed was <0.75 m s⁻¹ were excluded from the comparison as, with limited mixing of the atmosphere under more stable conditions, the air sampled by the in situ analyser did not necessarily represent the air in

the OP-FTIR measurement path. NH_3 is not measured by the in situ analyser and is difficult to calibrate. OP-FTIR CO , CO_2 and CH_4 data were corrected to the calibrated in situ data (linear regression: $N = 8700$; $r^2 = 0.98, 0.97, 0.97$ respectively).

Table 5. Detection limits and RMS for OP-FTIR for selected species determined as one std dev of 5-min measurements made under turbulent atmospheric conditions. Detection limits are defined as $3 \times \text{RMS noise}$.

Target Gas Species	Background	RMS Noise	** % Background	* Detection Limit
CO_2 (ppmv)	~400	0.7	0.2	2 ppmv
CO (ppbv)	~50	~2	4	6 ppbv
CH_4 (ppbv)	~1820	~2	0.1	6 ppbv
NH_3 (ppbv)	~2	0.3	15	1 ppbv

* $3 \times \text{RMS noise}$; ** RMS noise relative to the background mixing ratio for each gas.

3.4. Measured Mole-Fractions

Levels of NH_3 , CO , NO_x and SO_2 were lower during summer (October to March) compared with winter (May to September). During summer, NH_3 varied between 1.5 and 8 ppbv, with occasional excursions to 15 ppbv, when wind speeds were low (5-min average OP-FTIR data 3.1 ± 1.7 ppbv, $N = 30,945$), compared to winter when NH_3 ranged from 1–20 ppbv, with occasional excursions of 30 to 60 ppbv (average 4.2 ± 3.2 ppbv, $N = 29,551$). Minimum levels of CO during winter and summer were ~45 ppbv and reached a maximum ~800 ppbv in summer (average 149.0 ± 101 ppbv, $N = 30,943$) compared with ~2000 ppbv (average 320 ± 295 ppbv, $N = 29,553$) in winter (see Figure A3 for comparison of summer and winter levels of NH_3 and CO). NO_x levels (hourly average) were between a minimum level of 1–2 ppbv to 60–80 ppbv in summer, with occasional excursions up to 120 ppbv (14.5 ± 14.8 ppbv, $N = 2476$) and in winter 150–180 ppbv with occasional excursions to 300 ppbv (39.6 ± 42.8 , $N = 2286$). SO_2 (hourly average) varied from 0 to 5 ppbv in summer (0.55 ± 0.95 ppbv, $N = 3136$) and from 0 to 6 ppbv (0.76 ± 0.88 ppbv, $N = 2563$) in winter (see Figure A4, for a time-series comparing NH_3 , SO_2 and NO_x levels). CH_4 levels measured here under turbulent condition were ~1840 ppb and increased to over 4000 ppb during winter and 3500 ppb during summer (compared to 1776 ppbv in February 217 and 1816 ppbv in July 2017, at Cape Grim Baseline Air Pollution Station [48]).

Wind speed and associated atmospheric stability, was the major driver of the measured mole-fraction of the gases, with maximum levels typically at night, when the atmospheric conditions were stable, decreasing during the day as wind speeds and temperatures increased (Figure 5, winter data only shown). Independent of wind speed NH_3 , CO and NO_x levels decreased through the early hours until ~6:00 am when levels increased, reaching a maximum between 8:00 and 9:00. This was followed by a minimum, between 12:00 and 16:00, with a second maximum between 18:00 and 20:00. The timing of the maxima coincided with peak traffic (Figure A2). Corresponding maxima were not evident for CH_4 , with CH_4 levels plateauing around midnight, with a slower decrease between 8:00 and 14:00 and a steady increase from 18:00, consistent with changes in wind speed and atmospheric stability. This suggests an alternate source for CH_4 , with limited variability in the emission rate over the day. CH_4 , in the urban atmosphere, has been attributed to leaks in the domestic natural gas supply infrastructure, with spikes in emissions noted in the evening, associated with cooking and heating [49]. The source of the CH_4 is being investigated and will be reported in a future publication.

NH_3 in the atmosphere preferentially neutralises H_2SO_4 over HNO_3 , with a molar ratio of 2:1, for the formation of ammonium sulphate ($(\text{NH}_4)_2\text{SO}_4$) particulate matter (PM). From the mole-fractions measured here, excess NH_3 was available to neutralise SO_2 , with the formation of $(\text{NH}_4)_2\text{SO}_4$ being SO_2 limited. In contrast, for NO_x , there was insufficient NH_3 available to neutralise all potential HNO_3 and the formation of NH_4NO_3 was NH_3 limited. NH_3 levels were on average 33% of NO_x , with NH_3 exceeding NO_x for only 2% of the measurement time. From these data ~25% of the NH_3 will form $(\text{NH}_4)_2\text{SO}_4$ with 75% available for the formation of NH_4NO_3 . If the S in Australian fuels

is decreased (from the current level of 150 ppb, for the most commonly used fuel, to a proposed 10 ppb), the accompanying increase in the performance of the 3-way catalytic converter will result in a greater proportion of the NO being reduced to NH₃. However, with the potential decrease in NO and increase in NH₃ levels, it is difficult to predict changes to NH₄NO₃ inorganic PM production, as the environmental influences on the production of NH₃NO₃ are complex.

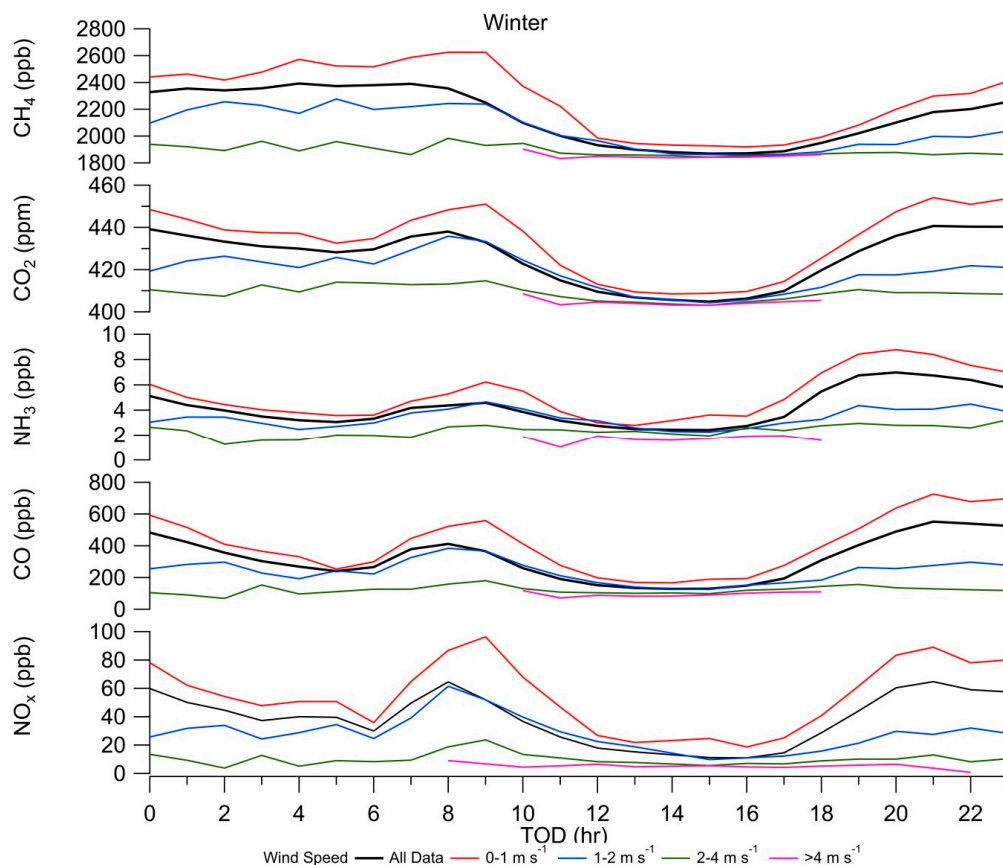


Figure 5. The variation in CH₄ (ppbv), CO₂ (ppbv), NH₃ (ppbv), CO (ppbv) and NO_x (ppbv) with the hour-of-day and binned to wind speeds 0–1 m s^{−1}, 1–2 m s^{−1}, 2–4 m s^{−1}, >4 m s^{−1} and averaged for all wind speeds (winter). CH₄, CO₂, NH₃ and CO were measured by the open-path FTIR, while NO_x was measured at the Mobile Air Quality (MAQ) station.

3.5. Ratio to CO

Prior to analysis, data were filtered for wind speed > 0.5 m s^{−1}, to remove data collected under very stable atmospheric conditions. This removes data where the CO and NH₃ have been decoupled during transport to the line sensor, as the frequency and characteristics of turbulence cells become more erratic with increasing stability [34,36]. The longer transport times to the sensor can also promote greater deposition of NH₃. This filtering removed 15% of the data during summer, of which nearly 80% was during the night (18:00 to 6:00). In winter 20% of data were removed, with 75% during the night.

The relationship of NH₃ and NO_x with CO was determined based on a weighted orthogonal distance regression (WODR) [50] as described by Wu and Yu 2018 [51]. In this work, the uncertainties in the two variables of the regression (NH₃ or NO_x and CO) were similar and an ordinary least squares regression, which assumes uncertainties only in the dependent variable, was deemed inappropriate. The WODR weights the points in the regression, based on the uncertainty in the x and y data for the regression, minimising the sum of squared orthogonal distance, from the data points to the regression line [50]. Wu and Yu 2018 compared several regression techniques, and, based on this analysis, WODR was deemed the most appropriate for the data uncertainties in this work.

For analysis, data were divided into periods encompassing the morning and afternoon peak traffic, weekend and weekdays and wind direction for the 4 sectors of the compass (northeast 0°–90°; southeast 90–180°; southwest 180–270°; northwest 270–360°; Table 6). As vehicle emissions are highly variable with driving conditions, vehicle fleet and environmental conditions, NH₃:CO and NO_x:CO were further calculated for each hour-of-day, for weekend and weekday, to capture changes at higher temporal resolution (Figures 6 and 7).

The comparison of CO with NH₃ for all data (wind speed > 0.5 m s⁻¹) showed good correlations for both seasons, with r², from the regression, of 0.63 and 0.60 (NH₃:CO summer and winter; Table 6). The correlation between NH₃ and CO was strongest during the morning and afternoon mole-fraction maxima (Table 6).

Table 6. The ratio of the measured NH₃ (ppbv) to CO (ppbv) derived from the slope (±standard error of the estimate) and r² of the weighted orthogonal distance regression (WODR). N is the number of points used in the regression.

Summer	NH ₃ :CO ppbv:ppbv	r ²	N	NO _x :CO ppbv:ppbv	r ²	N
all	0.0197 ± 0.0002	0.63	2260	0.120 ± 0.001	0.73	1573
AM	0.0180 ± 0.0003	0.68	461	0.154 ± 0.003	0.83	334
PM	0.0219 ± 0.0004	0.62	533	0.0941 ± 0.0021	0.67	386
NE	0.0167 ± 0.0007	0.51	488	0.147 ± 0.003	0.80	720
SE	0.0146 ± 0.0004	0.60	988	0.100 ± 0.005	0.53	366
SW	0.0112 ± 0.0004	0.57	473	0.101 ± 0.003	0.60	638
NW	0.0109 ± 0.0005	0.53	380	0.127 ± 0.004	0.75	311
Weekend	0.0213 ± 0.0004	0.55	640	0.0700 ± 0.0018	0.54	327
Weekdays	0.0193 ± 0.0002	0.64	1620	0.125 ± 0.001	0.75	1246
Winter						
all	0.0111 ± 0.0001	0.60	1971	0.132 ± 0.001	0.71	1650
AM	0.0087 ± 0.0001	0.51	448	0.140 ± 0.002	0.69	390
PM	0.0200 ± 0.0004	0.79	374	0.129 ± 0.003	0.82	344
NE	0.0207 ± 0.0018	0.62	84	0.163 ± 0.016	0.58	78
SE	0.0138 ± 0.0006	0.73	170	0.060 ± 0.008	0.32	132
SW	0.0074 ± 0.0002	0.70	687	0.121 ± 0.003	0.77	585
NW	0.0066 ± 0.0002	0.54	966	0.120 ± 0.003	0.66	858
Weekend	0.0086 ± 0.0001	0.57	552	0.0984 ± 0.0013	0.7	514
Weekdays	0.0122 ± 0.0001	0.63	1419	0.158 ± 0.001	0.78	1136

Summer: October 2016 to March 2017; Winter: May 2017 to September 2017. Data is filtered for wind speeds >0.5 m s⁻¹. AM Summer: 5:00 to 9:00; Winter 6:00 to 10:00 am PM Summer 15:00 to 19:00; Winter 16:00 to 20:00. NE: 0–90°; SE: 90–180°; SW: 180–270°; NW:270–360°. Weekday: Monday to Friday; Weekend: Saturday Sunday.

NH₃:CO, derived from the slope of the regression (Table 6), varied considerably between summer and winter, time-of-day (morning and evening maxima), day of week (weekend and weekday) and with wind sector, ranging from 0.007 to 0.022 ppbv/ppbv. The mean and standard deviation of all winter values (0.0111 ± 0.0001) were close to half for those for all summer (0.0197 ± 0.0002), with the difference greatest during the morning peak times. From the variation in NH₃:CO with hour-of-day (Figure 6) these low NH₃:CO in winter are driven by very low values, <0.01, overnight between ~22:00 and 9:00. These data are also associated with weak correlations (<0.6) between NH₃ and CO. These low values overnight and into the early morning, were not evident during the summer evenings. During the middle of the day, NH₃:CO was similar in summer and winter (summer ~0.030, winter 0.027, Figure 6) and associated with strong correlations (0.6 to >0.8). Excluding these very low values during the early morning maxima, NH₃:CO ratio was greater during the afternoon maxima, compared to the morning maxima and greater on weekends compared to weekdays.

As NO_x is predominantly produced by diesel vehicles, NO_x:CO can be used as a tracer for diesel emissions. The correlation between NO_x and CO was good to strong with r² between 0.6 and 0.8. NO_x:CO was similar during winter and summer daytime, but, as with NH₃:CO, was lower at night during the winter. From the regression by the hour-of-day (Figure 7) during winter evenings NO_x:CO decreased to ~0.12 and remained low until ~8:00 am. In summer NO_x:CO initially decreased in

the early evening but increased from ~20:00, remaining elevated (0.15 and 0.20) until late morning. On weekdays, $\text{NO}_x:\text{CO}$ was highest during the am, measured maxima and into the middle of the day, decreasing in the afternoon and into the pm maxima (~0.01). On weekends $\text{NO}_x:\text{CO}$ was significantly reduced and remained low over the day (<0.12) with a corresponding weak correlation between NO_x and CO (typically <0.6).

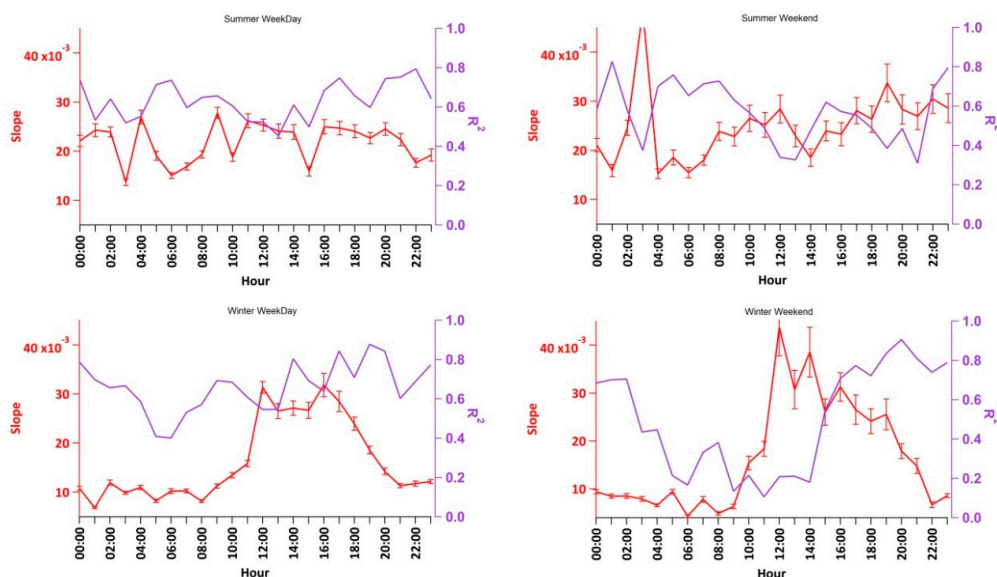


Figure 6. The Slope and r^2 value from the regression (WODR) between NH_3 and CO varied with the hour-of-day, for weekdays and weekends during summer (top panel) and winter (lower panel).

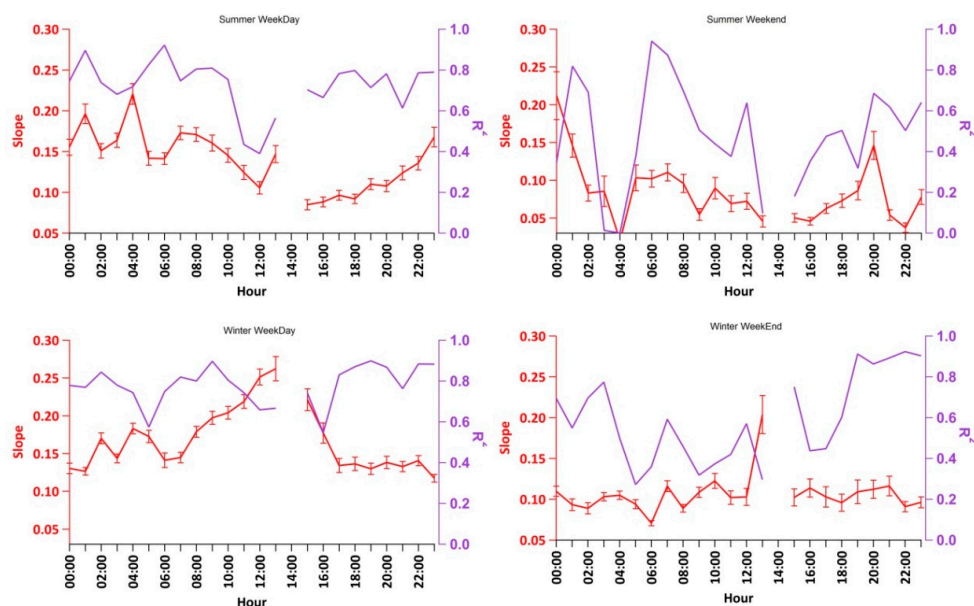


Figure 7. The Slope and r^2 value from the regression (WODR) between NO_x and CO varied with the hour-of-day, for weekdays and weekends during summer (top panel) and winter (lower panel). Data is missing at 14:00 due to daily instrument calibration.

The low $\text{NH}_3:\text{CO}$ and $\text{NO}_x:\text{CO}$ molar ratios, noted in the winter evenings and early mornings, may be due to the increased production of CO by domestic wood-burning heaters. During the cooler winter evenings, sharp increases were noted in 5-min averaged CO and NH_3 data, with corresponding increases in $\text{PM}_{2.5}$ and PM_{10} evident, indicative of wood smoke. Domestic wood burning stoves are a popular form of heating in southern Australia and has been shown to be a major contributor to PM_{10}

levels in winter, particularly in regional areas but also a substantial contribution to PM in Australian non-tropical cities [2]. It has been reported that, in 2014, domestic wood-smoke was responsible for up to 75% of PM_{2.5} and 57% of PM₁₀ in Sydney, during July, the coldest month in Sydney [52].

While domestic wood heaters are regulated (as of 1 November 2016, 55% efficiency and 2.5 g particulate emissions per kg wood burnt) emissions are expected to be higher as many wood heaters are thought to be operated inefficiently. The emission factor for NH₃ to CO, reported for domestic wood heaters, is less than that of petrol vehicles, with the NH₃:CO for molar emissions reported to be 0.0134 [53]. However with inefficient operation of wood heaters this will be reduced. An emission factor for NH₃ to CO for smoke events, identified in these data by the correlation with increased PM_{2.5} and PM₁₀, has been calculated as 0.009 ± 0.003 [45]. While NH₃ increased from an average 3.1 ppb in summer to 4.2 ppb in winter, CO increase from an average 149 ppb to 320 ppb from summer to winter. This represents a 35 % increase, from summer to winter, for NH₃, compared to a 115% increase in CO. With the inversions experienced during the cooler winter nights, CO will build in the atmosphere overnight, while the stable atmospheric conditions facilitates an increase in the rate of NH₃ deposition. From Figure 8, these increases in NH₃ and CO levels overnight, during winter, are less evident as the wind speed increased, typically mid-morning (~9:00). During summer nights, the increased NH₃ and CO levels, with low wind speeds, was less and often dissipated during the early hours of the morning, meteorology dependent.

Increased NH₃:CO and decreased NO_x:CO, has been reported to be related to an increased proportion of petrol versus diesel vehicles. The higher NH₃:CO and lower NO_x:CO, during the afternoon compared to morning and weekends compared to weekdays, reflected the proportion of heavy diesel to light petrol vehicles on the nearby major roads (Table 1; Figure A2) [30]. The number of heavy vehicles, during the afternoon peak traffic, was ~ 50% of the morning peak traffic periods and 60% and 75% less on weekends, compared to weekdays, (Figure A2) with most commercial diesel vehicles operating between ~6:00 and 15:00 on weekdays and mostly off the road on weekends.

NH₃:CO was highest with winds from the northeast and southeast, towards the major roads and low to the southwest, toward the residential area, particularly in winter. In contrast, NO_x:CO was greatest with winds from the northeast and northwest and lowest with winds from the south. The higher NH₃:CO and NO_x:CO, measured from the north-eastern sector, was potentially associated with vehicle emissions from the frequently congested intersection to the north-east, together with emissions from the A44 and M4. The low NH₃:CO, from the southwestern sector, towards the mainly residential sector, during winter, may be associated with the use of domestic wood heaters, as outlined previously.

The low NO_x:CO and high NH₃:CO, from the southeast sector, may be due to the line sensor (NH₃ and CO) and the point sensor (NO_x) sampling different plumes. With winds from the southeast, the NO_x point-sensor will only intercept the plume from the southern section of the A6, 300–800 m from the measurement site and did not sample the plume from the M4 motorway or A44. However, the line-sensor, measuring NH₃ and CO, continued to sample plumes originating from the A6, A44 and M4 motor way. This may account for the difference in NH₃:CO and NO_x:CO from the southeast sector.

From the comparison of molar-ratio with wind direction (Figure A5), higher levels of NH₃ were noted in sector ~270° to 25° but with close to background levels from sector ~180°–135°, except when wind speeds were low. There was also evidence for an increase CO and NO_x levels from the north-west sector. During both winter and summer, the correlation between CO and NH₃ was weakest from the northern sector and the intercept of the regression was also significantly higher for NH₃ from the western sector (1.5 and 2.2 ppbv compared with 0.8 and 0.6 ppbv; data not shown), which may indicate additional non-correlated emission sources of NH₃ and CO. Increased levels of SO₂, NO_x and CO were noted from the east and southeast. CH₄ levels were close to background for most sectors except between 225 to 315 degrees where levels were increased, most likely associated with the residential area and possible leaks from the domestic natural gas reticulation system.

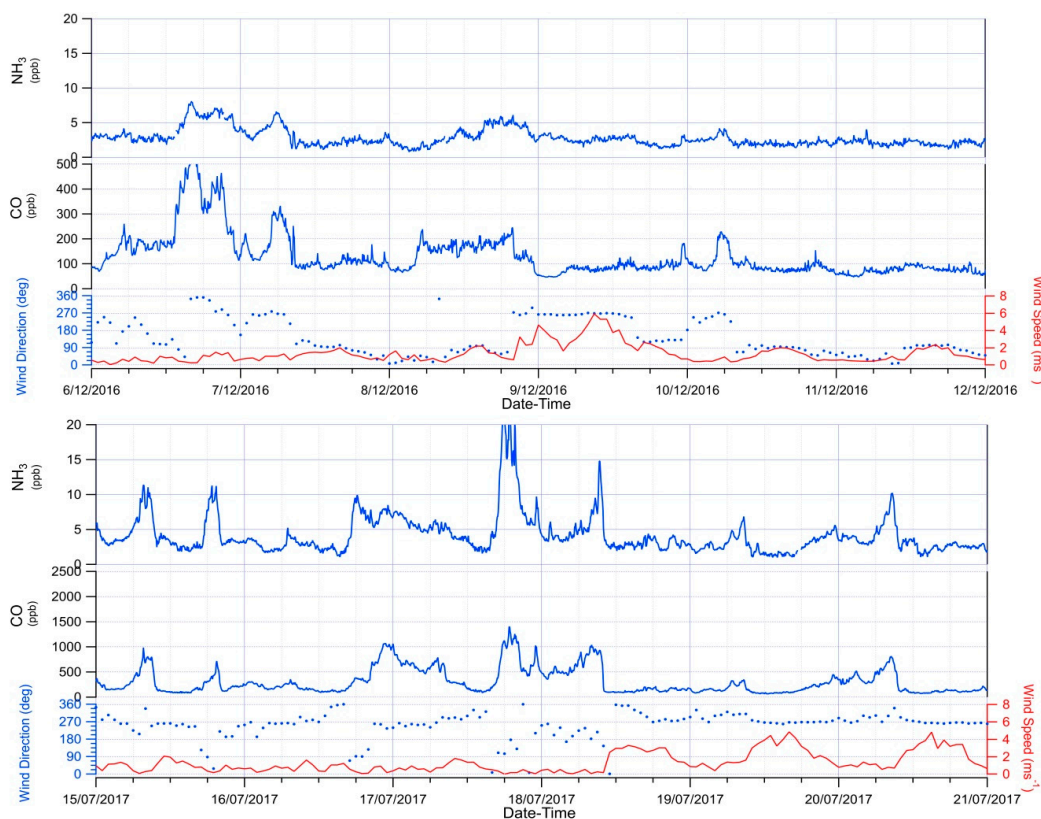


Figure 8. The time series, over 6 days, for CO and NH₃ and the corresponding wind speed (m s^{-1}) and direction ($^{\circ}$) during winter (top panel) and summer (lower panel) illustrates the increases in NH₃ and CO levels overnight, during winter, which dissipates as wind speed increases, typically during the morning between 6:00 and 9:00. During summer, the increase in CO and NH₃, with low wind speed overnight, is less and dissipates in the early morning, before 6:00.

The Australian National Pollutant Inventory [54], reports there are significant industrial source of CO, NH₃ and NO_x to the north and west of the site. The city of Sydney and Sydney Harbor is 15 km to the east of the site and Port Botany, the major port for Sydney, is 20 km to the southeast. Details on these other emission sources are given in the Appendix A. Currently there is insufficient information available from this study to confirm contribution from the surrounding sources, however it is hoped this can be addressed in future work.

NH₃ levels measured in Auburn, Western Sydney (summer 1.5–8 ppb; winter 1–20 ppb) were similar to measurements in other major cities. For example, NH₃ levels of 0–23 ppbv were measured over a highway in Toronto, Canada (0–23 ppbv) [19], while near-road measurements in Raleigh, NC, USA, measured 10–35 ppbv [24] and 5.5 to 60 ppbv in Rome [22].

Table 7 presents a limited number of examples of NH₃:CO or NH₃:CO₂, measured in various cities. NH₃:CO ranges from 0.023, for over highway measurements in Toronto, to 0.061 for tailpipe measurements, while NH₃:CO₂ measurements ranging from 0.27 ppbv:ppmv, measured in a tunnel in Houston, to 0.56 ppbv:ppmv, for on-road measurements in Shijiazhuang.

The emission ratio is dependent on the grade of the road, the driving style, the age and make of the vehicle and the 3-way catalytic converter installed [15], plus the quality of the fuel and S content. For example, tunnels and on-ramps, where measurements are often made, can have a considerable grade, while an increase in the inclination of a road by 7% has been shown to double emissions [15,18]. This makes it difficult to compare results from different locations.

While the ratios measured here (NH₃:CO 0.018 to 0.219 ppbv:ppbv) are at the lower end of the range, this is not surprising. The emission ratio is closest to the measurements made in Toronto, Canada, over a major highway (0.023) [19]. Measurements were made using a very similar technique to here, with an

open-path FTIR measurement path spanning the highway. The conditions on the highway in Toronto appear similar to the M4, with a limited road gradient and constant speed with minimal acceleration. The mix of the driving styles, on the 3 major roads to the east of the site, will be dominated by steady velocity. The grades of these major roads are minimal. And, while the major intersection on the A6 (speed limit 70 km h⁻¹) leads to braking towards and acceleration away from the intersection, there was minimal acceleration on the A44, with predominantly slow moving traffic (speed limit 50 to 60 km h⁻¹) and traffic on the M4 (speed limit 90 km h⁻¹) was generally moving at constant speed, if slower during peak traffic times. S content of fuel, which is higher in Australia than many countries, has also been reported to reduce NH₃ emissions. While the lower efficiency of the catalytic converters, in the typically older vehicle fleet in Western Sydney, will also reduce the proportion of NO reduced to NH₃. In addition, in this work measurements were made some distance from the targeted roads, which can result in a loss of NH₃ and increased influence from other local sources.

Table 7. Comparison of measurements of vehicular emissions of NH₃:CO, NH₃:CO₂ and emission factors, including the location, type and duration of the measurements.

Location	Reference	Method; Duration	NH ₃ :CO ppbv/ppbv	NH ₃ :CO ₂ ppbv/ppmv	EF g kg ⁻¹ Fuel
Auburn	This work	OP-FTIR 34 weeks	0.018–0.022	0.23	0.25
Auburn	[53]	GMR2008 Inventory	0.015		
Toronto	[19]	OP-FTIR over highway; 2 weeks	0.023		
San Francisco	[18]	On-road, roadside, QCL, days	0.031 ± 0.005		0.49 ± 0.06
Los Angeles	[18]	On-road, QCL, 3 days	0.027		0.49 ± 0.06
Princeton	[18]	On-road, roadside, QCL, 3 days	0.029 ± 0.007		
Californian South Coast Basin	[9]	Airborne	0.031–0.038		
California	[10]	Tailpipe			0.46
Zurich, Switzerland	[55]	CRDS, On-road, 1 week			0.212
Tartu, Estonia	[55]	CRDS, On-road, 1 week			0.415
Tallinn, Estonia	[55]	CRDS, On-road, 1 week			0.199
Houston	[15]	On-road 18 h Tunnel City Wide		0.33 ± 0.05 0.27 ± 0.05 0.35 ± 0.04	
Denver	[15]	On-road. Open path sensor 17 h		0.40 ± 0.06	
Beijing	[15]	On-road Open path sensor 53 h		0.36 ± 0.05	
Baoding China	[15]	On-road Open path sensor 11 h 2013 On-road 2014		0.51 ± 0.08 0.43 ± 0.07	
Shijiazhuang	[15]	On-road, Open path sensor 7 h 2013 On-road 2014		0.48 ± 0.07 0.56 ± 0.08	
Los Angeles	[27]	roadside		0.49 ± 0.02	
Denver	[27]	roadside		0.38 ± 0.08	
West Los Angeles	[56]	tailpipe	0.061		
San Francisco	[20]	road tunnel 1999 road tunnel 2006		0.34 ± 0.02	0.64 ± 0.04 0.40 ± 0.02

3.6. Emission Factor

An emission factor, EF, for NH₃ per kg fuel consumed, can be calculated from the comparison of CO, CO₂ and NH₃ as [18]

$$EF = \left(\frac{\Delta NH_3}{\Delta CO_2 + \Delta CO} \right) \left(\frac{MW_{NH_3}}{MWC} \right) WC, \quad (5)$$

where MW_{NH₃} and MW_C are the molecular weight of the measured NH₃ and carbon (C) respectively and WC (0.85) is the fraction of C in the fuel by weight.

The correlation between CO₂ and CO was generally high (winter: r² = 0.8 to 1.0; summer: r² = 0.6 to 0.8), with CO₂:CO < 0.1 to 0.3 ppmv:ppbv in summer compared to <0.1 to 0.12 ppmv:ppbv in winter. (Table A1). CO₂:CO also differs from the eastern and western sectors, with the eastern sector lower in both seasons. The correlation between NH₃ and CO₂ was weaker, ranging from 0.4 to 0.8, with the NH₃:CO₂ ratio highest during the afternoon peak and lower during the morning peak. (Table 8).

An emission factor of 0.25 g kg⁻¹ fuel consumed was calculated based on the afternoon peak data, when the traffic is dominated by petrol passenger vehicles. This is similar to that measured in Zurich and Tallin, Switzerland [55] but low compared to that estimated in many other cities (Table 7).

Table 8. The ratio of the measured NH₃ (ppbv) and CO₂ (ppmv) derived from the slope (±standard error of the estimate) and r² of the WODR regression. N is the number of points used in the regression.

Summer	NH ₃ :CO ₂ ppb:ppm	r ²	N
all	0.088 ± 0.002	0.56	2664
WS > 0.5	0.094 ± 0.002	0.52	1866
AM	0.091 ± 0.003	0.73	353
PM	0.211 ± 0.012	0.52	307
Weekend	0.082 ± 0.004	0.45	556
Weekday	0.095 ± 0.002	0.53	1310
Weekend AM	0.084 ± 0.004	0.78	108
Weekday AM	0.09 ± 0.004	0.70	245
Winter	NH ₃ :CO ₂ ppb:ppm	r ²	N
all	0.094 ± 0.002	0.56	2482
WS > 0.5	0.076 ± 0.002	0.51	1971
AM	0.067 ± 0.003	0.53	448
PM	0.213 ± 0.01	0.69	223
Weekend	0.071 ± 0.003	0.52	552
Weekday	0.077 ± 0.002	0.51	1419
Weekend AM	0.06 ± 0.005	0.52	125
Weekday AM	0.066 ± 0.003	0.53	323

Summer: October 2016 to March 2017; Winter: May 2017 to September 2017. Data is filtered for wind speeds (WS) > 0.5 m s⁻¹. AM Summer: 5:00 to 9:00; Winter 6:00 to 10:00 am PM Summer 15:00 to 19:00; Winter 16:00 to 20:00. Weekday: Monday to Friday; Weekend: Saturday Sunday.

3.7. Comparison to GMR2008 Emissions Inventory

The Greater Metropolitan Region 2008 Inventory [53] is an air emissions inventory, for the NSW metropolitan regions, which encompasses biogenic, geogenic and anthropogenic sources. The inventory has a base year of 2008 and uses the baseline data to project emission estimates to 2036.

For the region encompassing the measurement site (33°51'11"; 151°2'7" point 10,994 of the inventory) the GMR2008 attributes petrol vehicle exhaust as the major, weekday, emission source for NH₃ (78%) and CO (85%). Minor emission sources include diesel vehicles, (NH₃ < 1% and CO 5%) plus other-sources (includes recreational vehicles and domestic lawn maintenance; NH₃ 21% and CO 7%). On weekends, other-sources dominant NH₃ emissions (other-sources 60%, petrol vehicle exhaust 40%) and are significant CO emission sources (other-sources 32%, petrol vehicle exhaust 63%). During winter, The GMR2008 attributes domestic wood heating as a significant source of NH₃ and CO emissions (18% and 22% of the total winter emissions), with maximum emissions during the winter afternoon and evenings (14:00 to 23:00) (Figure 9). The distribution, over the day, of NH₃, CO and NO_x

gaseous emissions, predicted by the GMR2008, was similar to the distribution measured in this work, with maxima in the morning (~7:00–8:00) and afternoon (~17:00–18:00) (Figure 9).

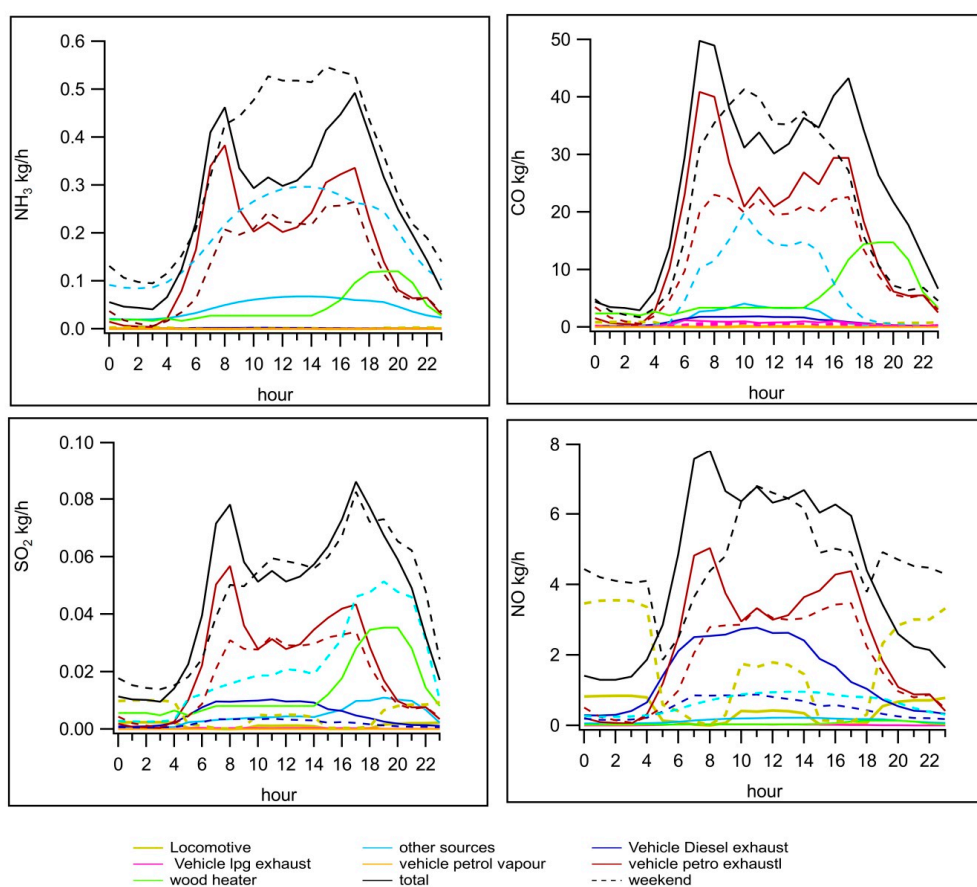


Figure 9. Emissions estimates and sources for NH_3 , CO, NO and N_2O from the GMR2008 inventory for 2017 at the measurement location [53].

For total emissions, the molar emissions ratio, NH_3 :CO, predicted by the GMR2008, was lower than the corresponding ratio we measured here (weekdays: measured, summer, NH_3 :CO 0.0193 ± 0.0002 ; inventory emissions NH_3 :CO 0.0147 ± 0.0009 , $r^2 = 0.81$; weekends: measured, summer, NH_3 :CO 0.0213 ± 0.0004 ; inventory emissions NH_3 :CO 0.0171 ± 0.0017 , $r^2 = 0.82$).

For emissions from petrol vehicles, the GMR2008 calculated the NH_3 :CO, for molar emissions, as 0.0153 ± 0.0008 , compared to 0.0180 ± 0.0003 and 0.0219 ± 0.0004 measured here for peak traffic times (am and pm respectively), when NH_3 and CO levels are dominated by petrol vehicles emissions. This suggests the GMR2008 may underestimate petrol vehicle NH_3 emissions, in 2017, by up to 50%. The GMR2008 predicts emissions in 2017 based on emissions in 2008. The NH_3 emissions in the GMR2008 were based on laboratory testbed emission estimates, which have been shown to underestimate NH_3 emissions [12]. In addition, post 2008, 3-way catalytic converter technology has improved, which can also contribute, in part, to the underestimation.

The GMR2008 uses a NH_3 :CO emissions factor for wood heaters of 0.134. However, as noted here previously, the emissions predicted by the GMR2008 during the winter evenings could not fully explain the very low NH_3 :CO, measured here at night (~0.01). This may be due domestic wood heaters operating at low efficiency and producing higher CO emissions, per kg wood burnt, than included in the inventory.

For total daytime emissions, NO_x :CO predicted by the GMR2008 and the measured NO_x :CO agreed well, with NO_x :CO emissions from the GMR2008 ranging from 0.12 to 0.2, compared with 0.070 to 0.16 for levels measured here. However, during the evening, the GMR2008 predicted emission ratios

increased, reaching 0.5 during week nights and up to 2.5 during nights on the weekend, due to the inclusion of high emissions from diesel locomotives a nights.

SO₂ contributes significantly to the formation of inorganic particulate matter in the urban atmosphere and changes in the S content of Australian fuels could potentially impact the formation of (NH₄)₂SO₄ particulate matter. The GMR2008 inventory identified petrol vehicle exhaust (66%) as the major source of SO₂ (Figure 9). Diesel vehicle exhaust contributed close to a 20% of the daytime, weekday, SO₂ emissions, with emissions decreasing by around 50% during the weekend, corresponding with the decreased numbers of diesel vehicles on the nearby roads. Other-sources contributed to SO₂ emissions during the evenings and were the dominant emission source during the evenings on weekends. During the winter afternoon and evenings, wood smoke was a substantial source of SO₂, contributing 20% of the total, winter emissions.

The GMR2008 inventory, for this region, includes substantial emissions of NO, NO₂ and SO₂, from freight diesel locomotives, contributing 3.5%, 9.5% and 6.2%, respectively, of the total, weekday emissions and 10%, 38% and 32%, respectively, on weekends (Australian, locomotive diesel oil contains 10 ppm S).

The number of rail freight movements increases as the frequency of commuter passenger trips decreases, including, during weekday off-peak commuter times, 10:00 to 14:00, weekday evenings and weekends. The GMR2008 predicts increased emissions during the weekday off-peak and evenings, with the highest emissions, predicted from diesel locomotives, during the weekends and maximum emissions during the nights of the weekend. From the log of freight train trips on the nearby rail line (May to September 2017) [57] the frequency of freight movements in 2017 was similar on weekends, weekday nights and during the daytime commuter off-peak periods, suggesting a change in the freight train timetable between 2008 and 2017. Identification of emissions from freight trains in these data has not been included here, as critical information was not available pre manuscript submissions. It is anticipated these data will be reported in a future publication.

4. Conclusions

An open path FTIR spectrometer simultaneously measured atmospheric NH₃, CO and CO₂ at high temporal resolution and high precision, over 11 months in Western Sydney, with the aims to assess the viability of OP-FTIR spectroscopy for long term measurements of urban air quality and quantify atmospheric NH₃ in an Australian urban environment. These data provide baseline measurements of NH₃ emissions prior to the possible decrease in S levels in Australian fuels. In addition NO_x and SO₂ were measured with an adjacent Mobile Air Quality station operated by the NSW Office of Environment and Heritage. The work was part of a larger project to investigate air quality in Western Sydney.

The OP-FTIR has proven to be a valuable tool in quantifying pollutants emitted in the urban environment, in particular NH₃, which can be difficult to measure. The simultaneous measurement of NH₃, CO and CO₂, at high temporal resolution and precision, over close to 12 months has provided the opportunity to compare emission at timescales of a day to a week and summer versus winter. For future work the instrument measurement precision could be improved further with modifications to the instruments beam expander and retroreflectors configuration.

The ratio of NH₃:CO was used as a tracer for vehicle NH₃ emissions while NO_x:CO was used as a tracer for diesel emission. The comparison of the two ratios provides a measure of relative emissions from petrol and diesel vehicles, while the relative levels of NH₃, NO_x and SO₂ provided data on the limitations to the formation of inorganic particulate matter. Emission estimates have been compared with the GMR2008 inventory.

NH₃ levels varied from 1 to 20 ppbv, CO from 45 to 2000 ppbv and NO_x from 1 to 300 ppbv and were higher during the winter than summer. SO₂ varied from 0 to 6 ppbv and was similar for both seasons. Based on these measurements, for the formation of (NH₄)₂SO₄ particulate matter, NH₃ was in excess and SO₂ was the limiting precursor. For the formation of NH₄NO₃ particulate matter, NH₃ was the limiting reagent with NH₃:NO_x typically ~0.3 This suggests any increase in NH₃ vehicle emissions, resulting from an increased efficiency of vehicle 3-way catalytic converters with a decreased

fuel sulphur content, has the potential to increase the formation of inorganic NH_4NO_3 . However the environmental factors influencing NH_4NO_3 formation are complex and the extent of NH_4NO_3 formation can be difficult to predict.

The ratio $\text{NH}_3:\text{CO}$, relating NH_3 production to combustion in vehicles, ranged between 0.0066 and 0.0219 ppbv/ppbv, with lower values measured during the winter evenings and into the early mornings. These low values were most likely due to domestic wood heaters providing an additional source of CO. $\text{NH}_3:\text{CO}$ molar ratio was greatest during the peak traffic hours, higher during the pm peak traffic than the am and higher on weekends than weekdays. In contrast $\text{NO}_x:\text{CO}$ was higher during the am than the pm peak traffic hours and higher during the week than on weekends, indicating the differences in the morning and evening ratios were driven by the relative number of diesel to petrol vehicles on the surrounding roads. From vehicle numbers on the nearby motorway there were 50% less heavy vehicles during the pm than am peak traffic hours and 60–75% fewer heavy vehicles on the roads during weekends compared to weekdays.

The GMR2008 predicted $\text{NH}_3:\text{CO}$ emissions ratio for petrol vehicles for 2017 is 0.0153 ± 0.008 which is significantly lower than $\text{NH}_3:\text{CO}$ measured in this study (0.022) during the afternoon peak traffic times, when emissions were dominated by petrol vehicles. The $\text{NO}_x:\text{CO}$ measured here was similar to the GMR2008 predicted emissions ratio. This suggests the GMR2008 emissions inventory may underestimate NH_3 vehicle emissions predicted for 2017. Inventory vehicle emission estimates are often based on test-bed emission measurements which have been shown to underestimate vehicle emissions under stop-start, uphill or aggressive motorway driving conditions. The average age of passenger vehicles in the area from the registration records is 10 years. Improvements in 3-way catalytic converter technology may have resulted in greater efficiency in reducing NO_x with a subsequent increase in NH_3 production.

This work contributes near-continuous data on emissions from motor vehicles that encompasses summer and winter environmental conditions with high temporal resolution and high precision. But it still only represents one location in one Australian city. It is hoped to expand this research and in particular to understand the influence on vehicle emissions with changing sulphur content in fuel. Machine learning is increasingly employed in tasks that require the detection of complex patterns, such as image analysis and in commerce. As the science develops, it can be expected that in the future, it will be able to address highly dimensional problem of predicting atmospheric circulation and pollution. Comprehensive data will contribute to this.

Author Contributions: The following authors contributed the following to the paper. The project was conceptualized by F.A.P., T.N., J.K., D.W.T.G. and C.P.-W.; The methodology was developed, the data validated and the formal analysis completed by F.A.P. and T.N.; Resources were provided by F.A.P., H.F. and D.W.T.G.; The first draft was written by F.A.P. and was reviewed and edited by T.N., H.F., C.P.-W. and D.W.T.G.; Software for the spectral analysis was written by D.W.T.G. The funding was acquired and the project administered by C.P.-W.

Funding: This research was supported by the Australian Government's National Environmental Science Program through the Clean Air and Urban Landscapes Hub.

Acknowledgments: The Authors would like to acknowledge the NSW Master Plumbers Association and the Auburn and Cumberland City Council for providing the locations for the measurement sites and to Mr Paul Naylor and Mr Douglas Greening of the NSW Master Plumbers Association for their technical assistance in the operation of the instruments. The authors also wish to acknowledge the work of the staff of the NSW Office of Environment and Heritage and EPA, in particular Mr Gunaratnam Gunashanhar, for the maintenance of the EPA Portable Monitoring Station, plus Doreena Dominick and Chris Caldwell, from the Centre for atmospheric Chemistry, for assistance with the maintenance of the spectrometers. We also acknowledge valuable discussion with Martin Cope on the GMR2008 inventory and for providing the relevant data from the GMR2008 and are grateful for the advice from Ian Galbally. The authors also wish thank the reviewers for their effort and contributions, which has substantially improved this manuscript.

Conflicts of Interest: The authors declare no conflict of interest. The funders had no role in the design of the study; in the collection, analyses or interpretation of data; in the writing of the manuscript or in the decision to publish the results.

Appendix A

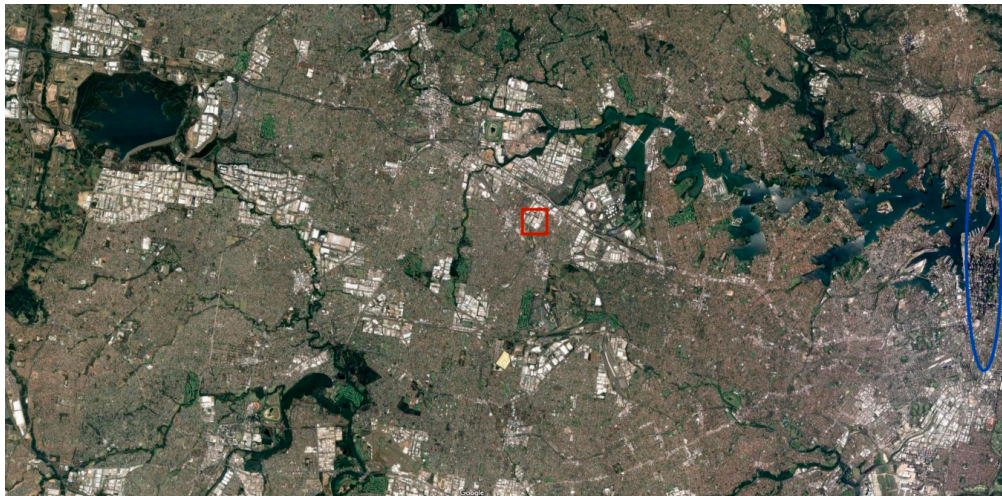


Figure A1. Map shows the location of the measurement site (□) within the Sydney greater area. For reference the Sydney Harbor Bridge is marked (○). The edge of the residential area and the start of agricultural areas can be seen on the east. It is 17 km from the measurement site to the Sydney Harbor Bridge.

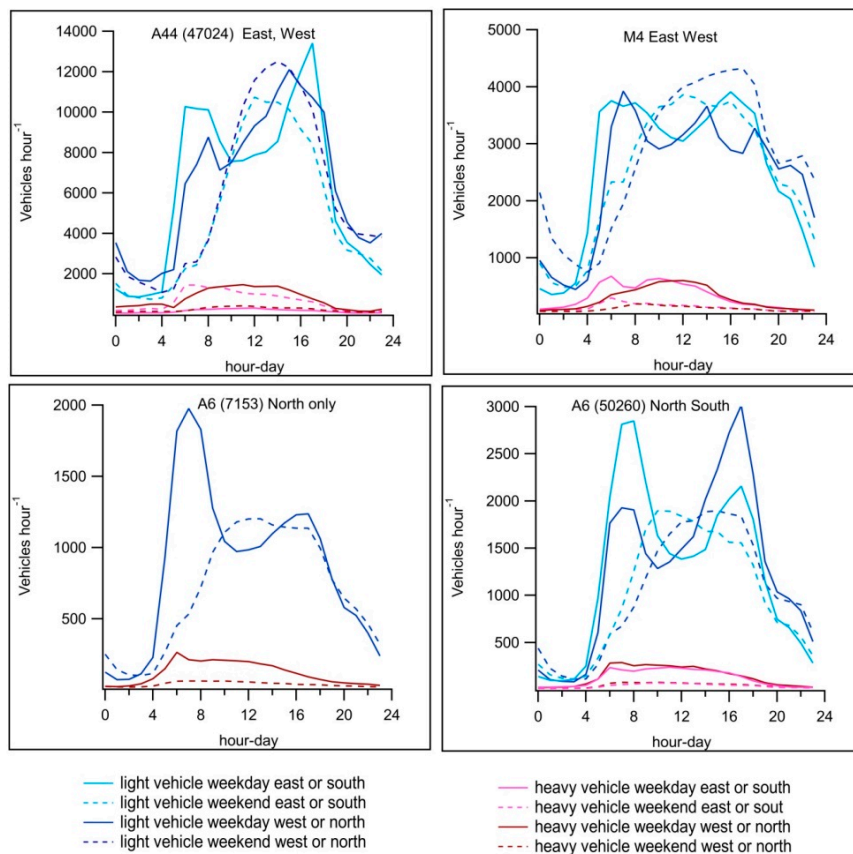


Figure A2. Traffic statistics sourced from camera counters on the A6, counter 7153 (north bound monitored only), 1 km north of the intersection on the A6 and 50,260 (monitoring north and south bound traffic), 3 km further north; the A44 (east and west bound traffic), counter 4701, 1.4 km from the A6/A44 intersection; The M4, monitoring east and west bound traffic) 1.8 km east of the A6/M4 interchange (2014–2015).

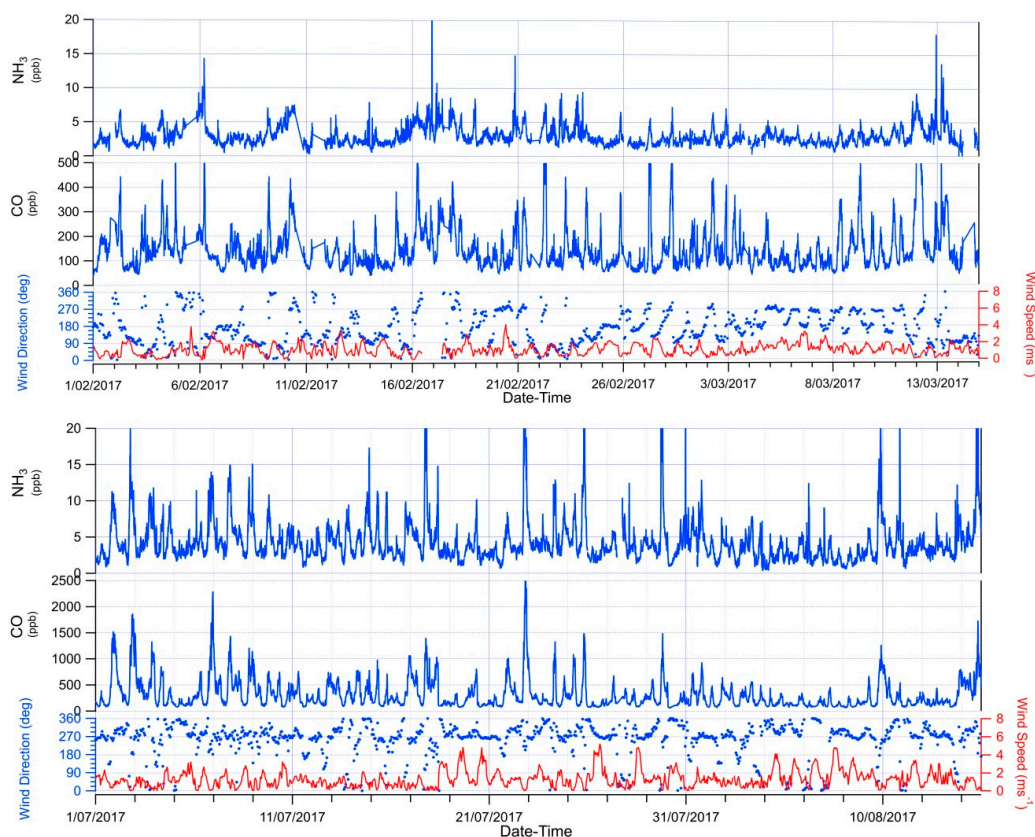


Figure A3. Time series of CO and NH₃ measured by the OP-FTIR system during summer (top panel) and winter (lower panel) in Western Sydney. Note the higher levels of CO and NH₃ measured in winter compared to summer. Wind speed (m s⁻¹) and wind direction are included in the lower panel of each plot.

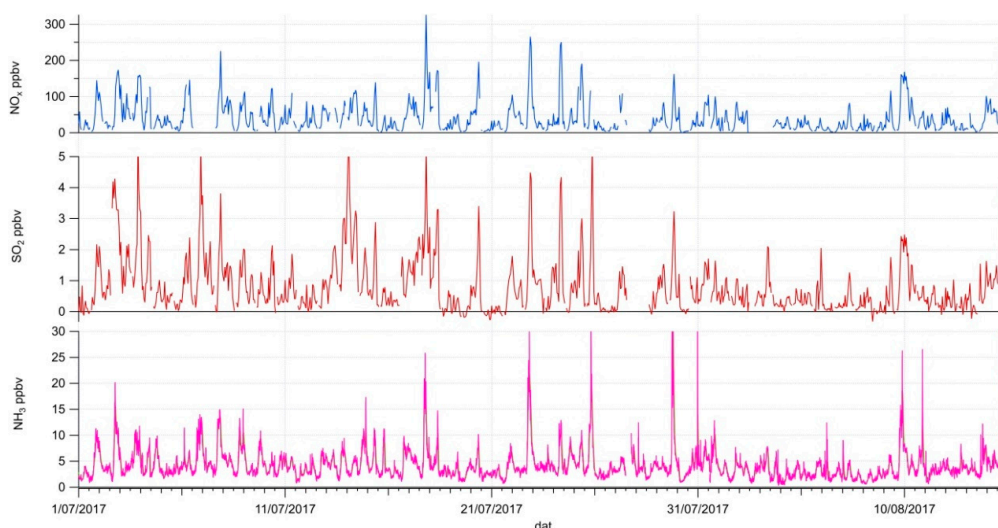


Figure A4. Time series comparing NH₃ measured by the OP-FTIR system and NO_x and SO₂ as measured at the Mobile Air Quality Station in Western Sydney.

Industrial Sources of NH₃, NO_x and CO

From the comparison of molar-ratio with wind direction (Figure A5), higher levels of NH₃ were noted in sector ~270° to 25° but with close to background levels from sector ~180°–135°, except when wind speeds were low. There was also evidence for an increase CO and NO_x levels from the north-west

sector. During both winter and summer, the correlation between CO and NH₃ was weakest from the northern sector and the intercept of the regression was also significantly higher for NH₃ from the western sector (1.5 and 2.2 ppbv compared with 0.8 and 0.6 ppbv; data not shown), which may indicate additional non-correlated emission sources of NH₃ and CO.

As reported in the Australian National Pollutant Inventory [54], there are significant industrial source of CO, NH₃ and NO_x to the north and west of the site,. These include a bitumen plant 3 km to the northwest (CO 12,700 kg year⁻¹, NO_x 8100 kg year⁻¹), a biscuit factory 15 km to the northwest, (the strongest local source of NH₃ 28,300 kg year⁻¹, CO 7300 kg year⁻¹), landfill electricity co-generation 25 km to the west (CO 59,500 kg year⁻¹, NO_x 150,000 kg year⁻¹) and 18 km to the northwest (CO 54 kg year⁻¹, NO_x 43,000 kg year⁻¹). Several biogenic sources were located to the west of the measurement site, including a sewage treatment plant (NH₃ 23,800 kg year⁻¹) 11 km to the southwest, a pork production farm 18 km to west (NH₃ 15,800 kg year⁻¹) and 3 poultry farms 20 to 25 km to the west (CO 10,000 kg year⁻¹, NH₃ 17,400 kg year⁻¹ and NO_x 11,000 kg year⁻¹). However, as the correlation between NH₃ and air temperature was low ($r^2 = 0.03$) and with the distance between these sources and the site (>10 km), these biogenic sources are thought unlikely to account for the additional NH₃. A brewery is listed located ~800 m to the northeast (NH₃ 6735 kg year⁻¹, CO 31,200 kg year⁻¹, NO_x 150,000 kg year⁻¹) which may contribute to the levels measured at the site from the northeast. But, from Figure A5, levels of the 3 gases to the northeast are low, with little evidence for a major source in the sector.

Increased levels of SO₂, NO_x and CO were also noted from the east and southeast. The city of Sydney and the harbor is 15 km to the east and Port Botany, the major port for Sydney, is 20 km to the southeast. Shipping to Sydney harbor includes cruise ships (344 visits in 2017) which dock either immediately east or west of the Harbor Bridge (smaller ships that fit under the Harbor Bridge), trade ships, predominantly bulk carriers (862 visits in 2017) that dock in the east of the harbor plus naval vessels. Container vessels and bulk oil carriers dock at Port Botany (total vessel visits 2016/2017, 1774), which is associated with substantial road transport in the area. Limited research (for example [58]) has indicated the emissions from the harbor operations can penetrate into Western Sydney and it is possible the increase in SO₂, NO_x and CO to the east originated from operations around Sydney harbor.

CH₄ levels were close to background for most sectors except between 225 to 315 degrees where levels were increased, most likely associated with the residential area and possible leaks from the domestic natural gas reticulation system.

Currently there is insufficient information available from this study to confirm contribution from the surrounding sources, however it is hoped this can be addressed in future work.

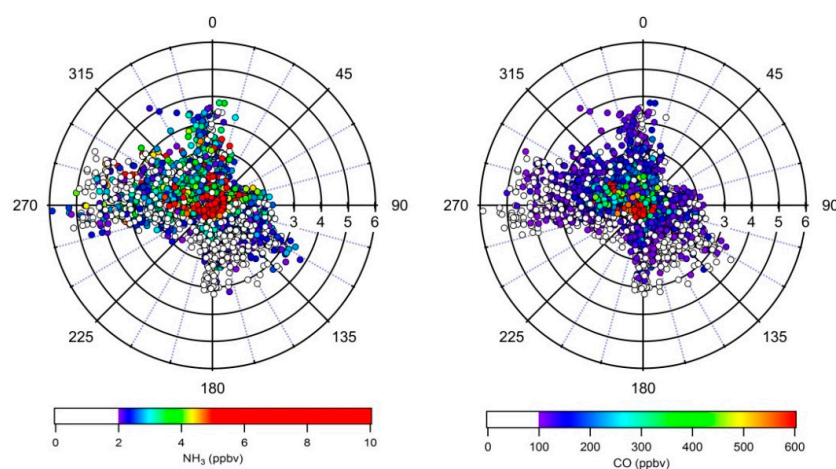


Figure A5. Cont.

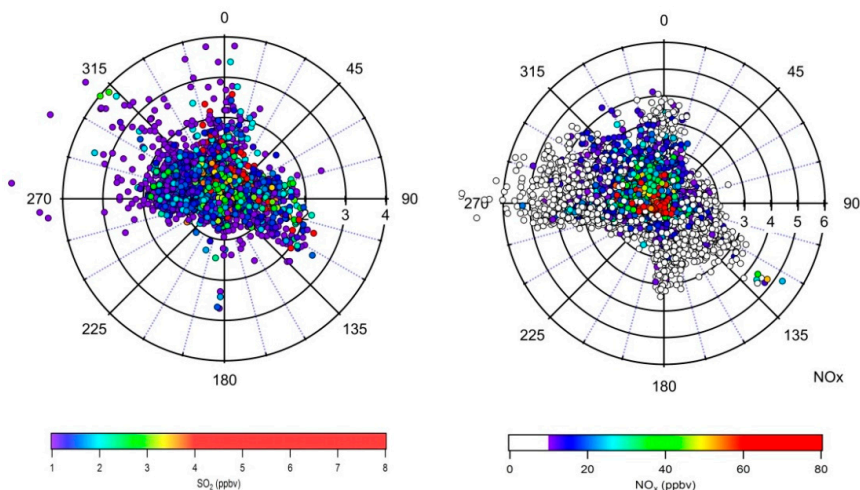


Figure A5. Polar bivariate plots for NH₃ (ppbv, top left panel), CO (ppbv, top right panel), SO₂ (ppbv, lower left panel) and NO_x (ppbv, lower right panel) NH₃ and CO were measured by the OP-FTIR between October 2016 and September 2017. NO_x and SO₂ were measured at the MAQ station between May 2016 and September 2017. For clarity, values close background (NH₃ < 2 ppbv, CO < 100 ppbv and SO₂, NO_x < 10 ppbv) are designated as white markers, SO₂ < 1ppbv removed and high values set to maximum colour designation (NH₃ > 5 ppbv, SO₂ > 4 ppbv, CO > 600 ppbv and NO_x > 60 ppbv). The radial axis is the wind speed (CO, NH₃ and NO_x: 0–6 m s⁻¹; and for clarity SO₂ 0–4 m s⁻¹).

Table A1. The ratio of the measured CO₂ to CO (ppbv) derived from the slope (\pm standard error of the estimate), the intercept (\pm standard error) and r² of the WODR regression. N is the number of points used in the regression.

Summer	CO ₂ :CO ppmv:ppbv	Intercept ppmv	r ²	N
all	0.172 ± 0.001	387.7 ± 0.1	0.66	2260
AM	0.168 ± 0.002	387.9 ± 0.2	0.76	461
PM	0.101 ± 0.002	391.0 ± 0.2	0.66	533
NE	0.083 ± 0.004	393.7 ± 0.6	0.46	488
SE	0.082 ± 0.002	394 ± 0.3	0.55	988
SW	0.123 ± 0.004	394.3 ± 0.8	0.65	473
NW	0.117 ± 0.005	394.2 ± 1.0	0.65	380
Weekend	0.217 ± 0.003	384.1 ± 0.2	0.65	640
Weekday	0.159 ± 0.001	388.8 ± 0.1	0.66	1620
Winter				
all	0.108 ± 0.0005	396.1 ± 0.1	0.84	1971
AM	0.103 ± 0.0010	399.0 ± 0.2	0.82	448
PM	0.0769 ± 0.0015	397.0 ± 0.2	0.88	374
NE	0.0503 ± 0.0059	403.5 ± 1.2	0.47	84
SE	0.0487 ± 0.0038	400.2 ± 0.5	0.49	170
SW	0.0786 ± 0.0013	400.5 ± 0.5	0.83	687
NW	0.0831 ± 0.0012	400.1 ± 0.4	0.82	966
Weekend	0.109 ± 0.001	395.0 ± 0.1	0.81	552
Weekday	0.108 ± 0.001	396.5 ± 0.1	0.86	1419

Summer: October 2016 to March 2017; Winter: May 2017 to September 2017. Data is filtered for wind speeds > 0.5 m s⁻¹. AM Summer: 5:00 to 9:00; Winter 6:00 to 10:00 am PM Summer 15:00 to 19:00; Winter 16:00 to 20:00. NE: 0–90°; SE: 90–180°; SW: 180–270°; NW:270–360°. Weekday: Monday to Friday; Weekend: Saturday Sunday.

References

1. Jalaludin, B.; Mannes, T.; Morgan, G.; Lincoln, D.; Sheppard, V.; Corbett, S. Impact of ambient air pollution on gestational age is modified by season in Sydney, Australia. *Environ. Health A Glob. Access Sci. Source* **2007**, *6*, 16. [[CrossRef](#)] [[PubMed](#)]
2. Denison, L. *Literature Review on the State of Knowledge of the Health and Environmental Impacts of Ambient Air Pollution in Australia*; Pacific Environment Limited: South Brisbane, Australia, 2015.
3. Marino, E.; Caruso, M.; Campagna, D.; Polosa, R. Impact of air quality on lung health: Myth or reality? *Ther. Adv. Chronic Dis.* **2015**, *6*, 286–298. [[CrossRef](#)]
4. Beer, T. Air quality as a meteorological hazard. *Nat. Hazards* **2001**, *23*, 157–169. [[CrossRef](#)]
5. Broome, R.A.; Fann, N.; Cristina, T.J.N.; Fulcher, C.; Duc, H.; Morgan, G.G. The health benefits of reducing air pollution in Sydney, Australia. *Environ. Res.* **2015**, *143*, 19–25. [[CrossRef](#)] [[PubMed](#)]
6. Crawford, J.; Chambers, S.; Cohen, D.D.; Williams, A.; Griffiths, A.; Stelcer, E.; Dyer, L. Impact of meteorology on fine aerosols at Lucas Heights, Australia. *Atmos. Environ.* **2016**, *145*, 135–146. [[CrossRef](#)]
7. Toro, R.A.; Canales, M.; Flocchini, R.G.; Morales, R.G.E.; Leiva, G.M.A. Urban atmospheric ammonia in Santiago city, Chile. *Aerosol Air Qual. Res.* **2014**, *14*, 33–44. [[CrossRef](#)]
8. Behera, S.N.; Sharma, M. Investigating the potential role of ammonia in ion chemistry of fine particulate matter formation for an urban environment. *Sci. Total Environ.* **2010**, *408*, 3569–3575. [[CrossRef](#)] [[PubMed](#)]
9. Nowak, J.B.; Neuman, J.A.; Bahreini, R.; Middlebrook, A.M.; Holloway, J.S.; McKeen, S.A.; Parrish, D.D.; Ryerson, T.B.; Trainer, M. Ammonia sources in the California South Coast Air Basin and their impact on ammonium nitrate formation. *Geophys. Res. Lett.* **2012**, *39*. [[CrossRef](#)]
10. Livingston, C.; Rieger, P.; Winer, A. Ammonia emissions from a representative in-use fleet of light and medium-duty vehicles in the California South Coast Air Basin. *Atmos. Environ.* **2009**, *43*, 3326–3333. [[CrossRef](#)]
11. Suarez-Bertoa, R.; Zardini, A.A.; Astorga, C. Ammonia exhaust emissions from spark ignition vehicles over the New European Driving Cycle. *Atmos. Environ.* **2014**, *97*, 43–53. [[CrossRef](#)]
12. Baum, M.M.; Kiyomiya, E.S.; Kumar, S.; Lappas, A.M.; Lord, H.C. Multicomponent Remote Sensing of Vehicle Exhaust by Dispersive Absorption Spectroscopy. 1. Effect of Fuel Type and Catalyst Performance. *Environ. Sci. Technol.* **2000**, *34*, 2851–2858. [[CrossRef](#)]
13. Fraser, M.P.; Cass, G.R. Detection of Excess Ammonia Emissions from In-Use Vehicles and the Implications for Fine Particle Control. *Environ. Sci. Technol.* **1998**, *32*, 1053–1057. [[CrossRef](#)]
14. Mejía-Centeno, I.; Castillo, S.; Fuentes, G.A. Enhanced emissions of NH₃, N₂O and H₂ from a Pd-only TWC and supported Pd model catalysts: Light-off and sulfur level studies. *Appl. Catal. B Environ.* **2012**, *119–120*, 234–240.
15. Sun, K.; Tao, L.; Miller, D.J.; Pan, D.; Golston, L.M.; Zondlo, M.A.; Griffin, R.J.; Wallace, H.W.; Leong, Y.J.; Yang, M.M.; et al. Vehicle Emissions as an Important Urban Ammonia Source in the United States and China. *Environ. Sci. Technol.* **2017**, *51*, 2472–2481. [[CrossRef](#)] [[PubMed](#)]
16. Heeb, N.V.; Zimmerli, Y.; Czerwinski, J.; Schmid, P.; Zennegg, M.; Haag, R.; Seiler, C.; Wichser, A.; Ulrich, A.; Honegger, P.; et al. Reactive nitrogen compounds (RNCs) in exhaust of advanced PM-NO_x abatement technologies for future diesel applications. *Atmos. Environ.* **2011**, *45*, 3203–3209. [[CrossRef](#)]
17. Heeb, N.V.; Forss, A.-M.; Brühlmann, S.; Lüscher, R.; Saxer, C.J.; Hug, P. Three-way catalyst-induced formation of ammonia—velocity- and acceleration-dependent emission factors. *Atmos. Environ.* **2006**, *40*, 5986–5997. [[CrossRef](#)]
18. Sun, K.; Tao, L.; Miller, D.J.; Khan, M.A.; Zondlo, M.A. On-road ammonia emissions characterized by mobile, open-path measurements. *Environ. Sci. Technol.* **2014**, *48*, 3943–3950. [[CrossRef](#)]
19. You, Y.; Staebler, R.M.; Moussa, S.G.; Su, Y.; Munoz, T.; Stroud, C.; Zhang, J.; Moran, M.D. Long-path measurements of pollutants and micrometeorology over Highway 401 in Toronto. *Atmos. Chem. Phys.* **2017**, *17*, 14119–14143. [[CrossRef](#)]
20. Kean, A.J.; Littlejohn, D.; Ban-Weiss, G.A.; Harley, R.A.; Kirchstetter, T.W.; Lunden, M.M. Trends in on-road vehicle emissions of ammonia. *Atmos. Environ.* **2009**, *43*, 1565–1570. [[CrossRef](#)]
21. Nowak, J.B.; Neuman, J.A.; Bahreini, R.; Brock, C.A.; Middlebrook, A.M.; Wollny, A.G.; Holloway, J.S.; Peischl, J.; Ryerson, T.B.; Fehsenfeld, F.C. Airborne observations of ammonia and ammonium nitrate formation over Houston, Texas. *J. Geophys. Res. Atmos.* **2010**, *115*. [[CrossRef](#)]

22. Perrino, C.; Catrambone, M.; Di Menno Di Bucchianico, A.; Allegrini, I. Gaseous ammonia in the urban area of Rome, Italy and its relationship with traffic emissions. *Atmos. Environ.* **2002**, *36*, 5385–5394. [[CrossRef](#)]
23. Fountoukis, C.; Nenes, A.; Sullivan, A.; Weber, R.; Van Reken, T.; Fischer, M.; MatÅas, E.; Moya, M.; Farmer, D.; Cohen, R.C. Thermodynamic characterization of Mexico City aerosol during MILAGRO 2006. *Atmos. Chem. Phys.* **2009**, *9*, 15. [[CrossRef](#)]
24. Baldauf, R.; Thoma, E.; Hays, M.; Shores, R.; Kinsey, J.; Gullett, B.; Kimbrough, S.; Isakov, V.; Long, T.; Snow, R.; et al. Traffic and Meteorological Impacts on Near-Road Air Quality: Summary of Methods and Trends from the Raleigh Near-Road Study. *J. Air Waste Manag. Assoc.* **2008**, *58*, 865–878. [[CrossRef](#)]
25. Bradley, K.S.; Brooks, K.B.; Hubbard, L.K.; Popp, P.J.; Stedman, D.H. Motor Vehicle Fleet Emissions by OP-FTIR. *Environ. Sci. Technol.* **2000**, *34*, 897–899. [[CrossRef](#)]
26. Australian Commonwealth Government. Vehicle Emissions Discussion Paper. Available online: <https://infrastructure.gov.au/roads/environment/forum/index.aspx> (accessed on 12 September 2018).
27. Bishop, G.A.; Stedman, D.H. Reactive Nitrogen Species Emission Trends in Three Light-/Medium-Duty United States Fleets. *Environ. Sci. Technol.* **2015**, *49*, 11234–11240. [[CrossRef](#)]
28. Phillips, F.; Naylor, T.; Paton-Walsh, C.; Gunashanhar, G.; Kirkwood, J.; Griffith, D.W.T.; Riley, M.; Scorgie, Y.; Guérette, E.-A. *Measurements of Trace Gases Relevant to Air Quality in Western Sydney, Australia, from May 2016 to September 2017 as Part of the Western Air Shed and Particulate Study for Sydney (WASPSS)*; PANGAEA: Bremen, Germany, 2017; Available online: <https://doi.org/10.1594/PANGAEA.884317> (accessed on 15 October 2018).
29. Australian Bureau of Statistics. Motor Vehicle Census. Available online: <https://www.abs.gov.au/ausstats/abs@.nsf/mf/9309.0> (accessed on 28 March 2019).
30. NSW Government, R.M.S. Traffic Volume Viewer. Available online: www.rms.nsw.gov.au (accessed on 15 December 2018).
31. Wiedemann, S.G.; Phillips, F.A.; Naylor, T.A.; McGahan, E.J.; Keane, O.B.; Warren, B.R.; Murphy, C.M. Nitrous oxide, ammonia and methane from Australian meat chicken houses measured under commercial operating conditions and with mitigation strategies applied. *Anim. Prod. Sci.* **2016**, *56*, 1404–1417. [[CrossRef](#)]
32. Phillips, F.A.; Wiedemann, S.G.; Naylor, T.A.; McGahan, E.J.; Warren, B.R.; Murphy, C.M.; Parkes, S.; Wilson, J. Methane, nitrous oxide and ammonia emissions from pigs housed on litter and from stockpiling of spent litter. *Anim. Prod. Sci.* **2016**, *56*, 1390–1403. [[CrossRef](#)]
33. Naylor, T.A.; Wiedemann, S.G.; Phillips, F.A.; Warren, B.; McGahan, E.J.; Murphy, C.M. Emissions of nitrous oxide, ammonia and methane from Australian layer-hen manure storage with a mitigation strategy applied. *Anim. Prod. Sci.* **2016**, *56*, 1367–1375. [[CrossRef](#)]
34. McGahan, E.J.; Phillips, F.A.; Wiedemann, S.G.; Naylor, T.A.; Warren, B.; Murphy, C.M.; Griffith, D.W.T.; Desservettaz, M. Methane, nitrous oxide and ammonia emissions from an Australian piggery with short and long hydraulic retention-time effluent storage. *Anim. Prod. Sci.* **2016**, *56*, 1376–1389. [[CrossRef](#)]
35. Bai, M.; Griffith, D.W.T.; Phillips, F.A.; Naylor, T.; Muir, S.K.; McGinn, S.M.; Chen, D. Correlations of methane and carbon dioxide concentrations from feedlot cattle as a predictor of methane emissions. *Anim. Prod. Sci.* **2016**, *56*, 108–115. [[CrossRef](#)]
36. Laubach, J.; Bai, M.; Pinares-Patiño, C.S.; Phillips, F.A.; Naylor, T.A.; Molano, G.; Cárdenas Rocha, E.A.; Griffith, D.W.T. Accuracy of micrometeorological techniques for detecting a change in methane emissions from a herd of cattle. *Agric. For. Meteorol.* **2013**, *176*, 50–63. [[CrossRef](#)]
37. Jones, F.M.; Phillips, F.A.; Naylor, T.; Mercer, N.B. Methane emissions from grazing Angus beef cows selected for divergent residual feed intake. *Anim. Feed Sci. Technol.* **2011**, *166–167*, 302–307. [[CrossRef](#)]
38. Feitz, A.; Schroder, I.; Phillips, F.; Coates, T.; Negandhi, K.; Day, S.; Luhar, A.; Bhatia, S.; Edwards, G.; Hrabar, S.; et al. The Ginninderra CH₄ and CO₂ release experiment: An evaluation of gas detection and quantification techniques. *Int. J. Greenh. Gas Control* **2018**, *70*, 202–224. [[CrossRef](#)]
39. Paton-Walsh, C.; Smith, T.E.L.; Young, E.L.; Griffith, D.W.T.; Guarett, E.A. New emission factors for Australian vegetation fires measured using open-path Fourier transform infrared spectroscopy—Part 1: Methods and Australian temperate forest fires. *Atmos. Chem. Phys.* **2014**, *14*, 24. [[CrossRef](#)]
40. Guerette, E.-A.; Paton-Walsh, C.; Desservettaz, M.; Smith, T.E.L.; Volkova, L.; Weston, C.J.; Meyer, C.P. Emissions of trace gases from Australian temperate forest fires: Emission factors and dependence on modified combustion efficiency. *Atmos. Chem. Phys.* **2018**, *18*, 19. [[CrossRef](#)]
41. Griffith, D.W.T. Synthetic Calibration and Quantitative Analysis of Gas-Phase FT-IR Spectra. *Appl. Spectrosc.* **1996**, *50*, 59–70. [[CrossRef](#)]

42. Griffith, D.W.T.; Deutscher, N.M.; Caldw, C.G.R.; Kettlewell, G.; Riggenbach, M.; Hammer, S. A Fourier transform infrared trace gas analyser for atmospheric applications. *Atmos. Meas. Tech. Discuss.* **2012**, *5*, 3717–3769. [[CrossRef](#)]
43. Griffith, D.W.T.; Pöhler, D.; Schmitt, S.; Hammer, S.; Vardag, S.N.; Platt, U. Long open-path measurements of greenhouse gases in air using near-infrared Fourier transform spectroscopy. *Atmos. Meas. Tech.* **2018**, *18*, 14. [[CrossRef](#)]
44. Rothman, L.S.; Jacquemart, D.; Barbe, A.; Chris Benner, D.; Birk, M.; Brown, L.R.; Carleer, M.R.; Chackerian, J.C.; Chance, K.; Coudert, L.H.; et al. The HITRAN 2004 molecular spectroscopic database. *J. Quant. Spectrosc. Radiat. Transf.* **2005**, *96*, 139–204. [[CrossRef](#)]
45. Desservettaz, M.; Phillips, F.; Naylor, T.; Paton-Walsh, C.; Price, O.; Kirkwood, J. Air quality impacts of smoke from hazard reduction burns and domestic wood heating in western Sydney. *Atmosphere* **2019**. Submitted.
46. Simmons, J.; Paton-Walsh, C.; Phillips, F.; Naylor, T.; Guerette, É.-A.; Graham, J.; Keatley, T.; Burden, S.; Dominick, D.; Kirkwood, J.; et al. Understanding Spatial Variability of Air Quality in Sydney: Part 1—A Suburban Balcony Case Study. *Atmosphere* **2019**, *10*, 181. [[CrossRef](#)]
47. Smith, T.E.L.; Wooster, M.J.; Tattaris, M.; Griffith, D.W.T. Absolute accuracy evaluation and sensitivity analysis of OP-FTIR NLS retrievals of CO₂, CH₄ and CO over concentrations ranging from those of ambient atmospheres to highly polluted plumes. *Atmos. Meas. Tech.* **2011**, *4*, 97–116. [[CrossRef](#)]
48. CSIRO. Cape Grim Greenhouse Gas Data. Available online: www.csiro.au/en/Research/OandA/Areas/Assessing-our-climate/Greenhouse-gas-data (accessed on 15 March 2019).
49. Kelly, B.F.; Iverach, C.P.; Lowry, D.; Fisher, R.E.; Frances, J.L.; Nisbet, E.G. Fugitive methane emissions from natural, urban, agricultural and energy-production landscapes of eastern Australia. In Proceedings of the EGU General Assembly 2015, Vienna, Austria, 12–17 April 2017. Geophysical Research Abstracts.
50. Carroll, R.J.; Ruppert, D. The Use and Misuse of Orthogonal Regression in Linear Errors-in-Variables Models. *Am. Stat.* **1996**, *50*, 1–6.
51. Wu, C.; Yu, J.Z. Evaluation of linear regression techniques for atmospheric applications: The importance of appropriate weighting. *Atmos. Meas. Tech.* **2018**, *11*, 1233–1250. [[CrossRef](#)]
52. EPA. Wood Smoke Isn't Good Smoke. Available online: <https://www.epa.nsw.gov.au/your-environment/air/reducing-wood-smoke-emissions> (accessed on 20 March 2019).
53. Environment Protection Authority. *Technical Report 1. Air Emissions Inventory for the Greater Metropolitan Region in NSW 2008*; Environment Protection Authority: Sydney, Australia, 2012.
54. Department of Environment and Energy, Australian Government. *National Pollution Inventory*; Australian Government: Canberra, Australia, 2018. Available online: www.npi.gov.au/npi-data (accessed on 12 October 2018).
55. Elser, M.; El-Haddad, I.; Maasikmets, M.; Bozzetti, C.; Wolf, R.; Ciarelli, G.; Slowik, J.G.; Richter, R.; Teinmaa, E.; Hüglin, C.; et al. High contributions of vehicular emissions to ammonia in three European cities derived from mobile measurements. *Atmos. Environ.* **2018**, *175*, 210–220. [[CrossRef](#)]
56. Bishop, G.A.; Peddle, A.M.; Stedman, D.H.; Zhan, T. On-Road Emission Measurements of Reactive Nitrogen Compounds from Three California Cities. *Environ. Sci. Technol.* **2010**, *44*, 3616–3620. [[CrossRef](#)]
57. Transport NSW. *Sydney Trains 2013 Standard Working Timetable, Rail Freight Services*; Books 4&5; State Government NSW: Sydney, Australia, 2013.
58. Abraham, J. *Emissions from Ships Operating in the Sydney Greater Metropolitan Area*; NSW Environment Protection Authority: Sydney, Australia, 2015.

